Preprint Cambridge Centre for Computational Chemical Engineering ISSN 1473 – 4273

On a multivariate population balance model to describe the structure and composition of silica nanoparticles

Shraddha Shekar [1], Alastair J. Smith [1], Markus Kraft [1], Wolfgang Wagner [2]

released: 5 August 2011

[1] Department of Chemical Engineering
and Biotechnology
University of Cambridge
New Museums Site
Pembroke Street
Cambridge, CB2 3RA
UK
E-mail: mk306@cam.ac.uk

[2] Weierstrass Institute for
Applied Analysis and Stochastics
Mohrenstraße 39
10117 Berlin
Germany
E-mail: wagner@wias-berlin.de

Preprint No. 105

Keywords: silica nanoparticle, population balance model, numerics, convergence

Edited by
Computational Modelling Group
Department of Chemical Engineering and Biotechnology
University of Cambridge
New Museums Site
Pembroke Street
Cambridge CB2 3RA
United Kingdom

Fax: + 44 (0)1223 334796
E-Mail: c4e@cam.ac.uk
World Wide Web: http://como.cheng.cam.ac.uk/

Abstract

The aim of this work is to present the mathematical description of a detailed multivariate population balance model to describe the structure and composition of silica nanoparticles. Silica nanoparticles are formed by the interaction of silicic acid monomers ($Si(OH)_4$)in the gas-phase. A detailed numerical study of a stochastic particle algorithm for the solution of the multidimensional population balance model is presented. Each particle is described by its constituent primary particles and the connectivity between these primaries. Each primary, in turn, has internal variables that describe its chemical composition, i.e., the number of Si, free O and OH units. A particle undergoes transformations due to different particle processes such as surface reactions, coagulation, sintering, and intra-particle reactions. The algorithms used to solve the population balance equations and to couple the population balance model to gas-phase chemistry are described. Numerical studies are then performed for a number of functionals calculated from the model to establish the convergence with respect to the numerical parameter that determines the number of computational particles in the system. A brief numerical investigation of convergence with respect to the splitting time step has also been undertaken. The computational times (for runs that provide acceptable statistical errors) are determined to be sufficiently small to facilitate the application of this detailed multidimensional model to simulate industrial scale systems.

Contents

1 Introduction

Silica nanoparticles play a vital role as functional materials in a variety of applications such as ceramics, catalysis, bio-imaging, bio-sensing and drug delivery. For sensitive applications, the synthesis of particles with highly specific properties, such as particle size, size distribution, and morphology is desired. To attain this, it is essential to understand the detailed mechanism of formation and growth of these nanoparticles. Previous studies on the flame synthesis of silica nanoparticles from tetraethoxysilane (TEOS) suggest the formation of nanoparticles via the interaction of silicic acid ($SiOH_4$) monomers [7, 18, 23]. This work aims to mathematically describe the particle formation mechanism in an unprecedented level of detail by tracking the evolution of the chemical units (Si, O and OH) in each particle in the ensemble.

The use of population balance modelling to study particle dynamics has received considerable attention in the last few decades. Hulburt and Katz [8] first presented a statistical mechanical formulation (referred to as population balance equations (PBEs)) for a class of problems in particle technology. A multitude of attempts have since been made to apply population balance modelling to further the understanding of particulate processes. The particle dynamics of flame-synthesised pyrogenic silica was first simulated by solving a one-dimensional population balance equation by Ulrich [28]. This work was further developed by Ulrich and Riehl [29] who detected the existence of particles as flocs or aggregates containing smaller primary particles and included this observation in the model by introducing an arbitrary shape-factor. Koch and Friedlander [9, 10] made an early attempt to describe particle growth in terms of coagulation and sintering, characterising an agglomerate not only by its volume, but also by its surface area. The one-dimensional approach was extended to two-dimensions by Xiong and Pratsinis [31] and Xiong et al. [32] who studied the formation of agglomerate particles by coagulation and sintering by solving the population balance equation using sectional methods to describe the evolution of both particle size and shape. Tsantilis et al. [27] used a similar approach to model the flame synthesis of titania nanoparticles. The growth of non-spherical silica particles in a counterflow diffusion flame was analysed by Lee et al. [12] where in addition to coagulation, they consider the effect of chemical reactions and coalescence. Morgan et al. [13] have extended this model to include particle inception, surface growth and sintering. Recently, more detailed particle models have been developed by Celnik et al. [3], Morgan et al. [14], Patterson and Kraft [16], Sander et al. [21] for soot modelling. The literature, however, remains sparse on detailed models to study inorganic nanoparticle systems.

Several numerical techniques exist for solving population balance equations. These techniques have been reviewed in detail by Ramkrishna and Mahoney [19] and Kraft [11]. Amongst these different solution techniques, the stochastic methods have been demonstrated to be efficient and offer a viable option to include further model detail on a particle level. Eibeck and Wagner [5] introduced stochastic particle algorithm known as the Direct Simulation Monte Carlo algorithm to solve the Smoluchowski coagulation equation. They used the technique of fictitious jumps using suitable majorant kernels. This algorithm was extended to include a source term for gas-phase reactions by Goodson and Kraft [6] and Balthasar and Kraft [1]. Patterson and Kraft [16] further refined this method by introducing a Linear Process Deferment Algorithm. Celnik et al. [2, 4] incorporated the effects

of gas-phase reactions into the stochastic population balance model by using an operator splitting technique, and West et al. [30] used such a coupled model to study the synthesis of titania particles. Despite being widely used in the past few decades, the performance of a multivariate stochastic model to study nanoparticle dynamics that includes various process transformations and is fully-coupled to the gas-phase chemistry, has never been explored in detail.

The main aim of this work is to present the mathematical formulation of a multidimensional stochastic population balance model fully coupled to a kinetic model that describes the evolution of chemical composition and structure of silica nanoparticles synthesised by high temperature decomposition of TEOS. Detailed numerical studies are then performed on the model to evaluate its convergence properties. The applications of this detailed model to study the problems related to chemical and process engineering are reported elsewhere [24].

The paper is structured as follows. In §2 we state the model mathematically with a brief description of the kinetic model in §2.1 and a detailed description of the stochastic particle model in §2.2. Each particle is represented in terms of its primary particles and the connectivity between these primaries as described in §2.2.1. Each primary particle, in turn, is described by its chemical composition *i.e.*, the number of Si, O and OH groups present in it. The type of the particles is altered due to several transformations such as surface reaction, coagulation, sintering and intra-particle reactions. The rates of each of these processes and their corresponding transformations are described in §2.2.2. The algorithms used to solve the population balance equations and to couple the PBEs to a gas-phase chemistry solver are presented in §2.3. Numerical studies performed on the model are reported in §3. A convergence study is performed with respect to different numerical parameters in the model in §3.3. The convergence speed of different functionals calculated from the model as well as the computational times are observed. The paper concludes with a discussion of the model's performance and suggests potential improvements to it, along with suitable steps for future research.

2 Model

The physical system modelled in this work is the gas-phase thermal decomposition of tetraethoxysilane ($Si(OC_2H_5)_4$) to form silica nanoparticles (SiNPs) through the global reaction:

$$Si(OC_2H_5)_4 \rightarrow \text{SiNP} + \text{Gas-phase species}.$$

The model consists of two parts: (i) a kinetic model describing the gas-phase processes; and (ii) a stochastic particle model describing the silica nanoparticle phase. These models are coupled using an operator splitting technique outlined in §2.3.1.

2.1 Kinetic Model

The overall gas-phase reaction that leads to the formation of the silicic acid precursor that ultimately form silica nanoparticles is given as:

$$\mathrm{Si(OC_2H_5)_4} \rightarrow \mathrm{Si(OH)_4} + 4\mathrm{C_2H_4}.$$

The silicic acid ($\mathrm{Si(OH)_4}$) monomers interact to eventually form silica nanoparticles through various particle processes described in §2.2.2.

The kinetic model for the decomposition of tetraethoxysilane used in this work is described in detail by Shekar et al. [23] and consists of 58 reversible gas-phase reactions and 27 chemical species. The system of reversible reactions involving N_g chemical species and I reactions can be represented in the general form:

$$\sum_{k=1}^{N_\mathrm{g}} \nu'_{ki}\chi_k \rightleftharpoons \sum_{k=1}^{N_\mathrm{g}} \nu''_{ki}\chi_k,$$

where ν'_{ki} and ν''_{ki} are the forward and reverse stoichiometric coefficients respectively of the k^{th} species of the i^{th} reaction where $i \in \{1, \ldots, I\}$. χ_k is the chemical symbol for the k^{th} species.

The production rate $\dot{m}_k$ of the k^{th} species can be written as a summation of the rate-of-progress variables for all reactions involving the k^{th} species:

$$\dot{m}_k = \sum_{i=1}^{I} \nu_{ki} q_i, \tag{1}$$

where

$$\nu_{ki} = \nu''_{ki} - \nu'_{ki}. \tag{2}$$

The rate of progress variable q_i for the i^{th} reaction is given by the difference of the forward and reverse rates as:

$$q_i = k_{f_i} \prod_{k=1}^{N_\mathrm{g}} [C_k]^{\nu'_{ki}} - k_{r_i} \prod_{k=1}^{N_\mathrm{g}} [C_k]^{\nu''_{ki}}, \tag{3}$$

where C_k is the molar concentration of the k^{th} species and k_{f_i} and k_{r_i} are the forward and reverse rate constants of the i^{th} reaction. The forward rate constants for the I reactions are assumed to have the following Arrhenius temperature dependence:

$$k_{f_i} = A_i T^{\beta_i} \exp\left(\frac{-E_i}{RT}\right), \tag{4}$$

where the pre-exponential factor A_i, the temperature coefficient β_i and the activation energy E_i are user specified and are listed for the current work in [23]. The reverse rate constants are determined from thermochemical data which are also provided as inputs.

The gas-phase chemistry is described by a set of N_g ODEs with the material balance of species k given by:

$$\frac{\mathrm{d}C_k}{\mathrm{d}t} = \dot{m}_k(C_k, T) + \dot{g}_k(C_k, N, T) - \gamma(C_k, T)C_k, \tag{5}$$

where C_k is the gas-phase concentration of the k^{th} species, $\dot{m}_k$ is the molar production rate of the k^{th} species due to gas-phase processes calculated in (1) and $\dot{g}_k$ the molar production rate due to particle processes described in §2.2.2. N is the number of particles in the system, T is the temperature of the system and γ is the rate of gas-phase expansion given by:

$$\gamma = \frac{\dot{m}_k(C_k, T)}{\rho} + \frac{1}{T}\frac{\mathrm{d}T}{\mathrm{d}t}, \tag{6}$$

where ρ is the molar density of the bulk fluid.

2.2 Particle Model

2.2.1 Type Space

Each particle is represented as:

$$P_q = P_q(p_1, \ldots, p_{n(P_q)}, \mathbf{C}). \tag{7}$$

Particle P_q consists of $n(P_q)$ primary particles p_i where $i \in \{1, \ldots, n(P_q)\}$. The state of the system is given by an ensemble of N particles of type P_q, $q \in \{1, \ldots, N\}$.

$\mathbf{C}$ is a lower diagonal matrix of dimension $n(P_q) \times n(P_q)$ storing the common surface between two primary particles and describes the sintering between them (details described in §2.2.2):

$$\mathbf{C}(P_q) = \begin{pmatrix} 0 & \cdots & 0 & \cdots & 0 \\ C_{21} & \ddots & 0 & \cdots & 0 \\ \vdots & \ddots & \ddots & \cdots & \vdots \\ C_{i1} & \cdots & C_{ij} & \ddots & \vdots \\ \vdots & \cdots & \vdots & \cdots & \vdots \end{pmatrix}. \tag{8}$$

The element C_{ij} of matrix $\mathbf{C}$ has the following property:

$$C_{ij} = \begin{cases} 0, \text{ if } p_i \text{ and } p_j \text{ are non-neighbouring}, \\ S_{\text{sph}}(p_i, p_j) \leq C_{ij} \leq s(p_i) + s(p_j), \text{ if } p_i \text{ and } p_j \text{ are neighbouring}. \end{cases} \tag{9}$$

where $S_{\text{sph}}(p_i, p_j)$ and $s(p_i)$, $s(p_j)$ are defined in (43) and (13) respectively.

Each primary p_i is described by internal variables $\eta_{\text{Si}}, \eta_{\text{O}}, \eta_{\text{OH}}$ as:

$$p_i = p_i(\eta_{\text{Si}}, \eta_{\text{O}}, \eta_{\text{OH}}) \tag{10}$$

where $\eta_x \in \mathbb{Z}$, $\eta_x \geq 0$ is the number of chemical units of type x, $x \in \{\text{Si}, \text{O}, \text{OH}\}$.

We define the following derived properties in terms of the internal variables:

- **Primary particle volume**: $v(p_i)$ of a primary p_i is calculated in terms of its chemical units as:

$$v(p_i) = \frac{(\eta_{\text{Si}}(p_i) \times M_{\text{Si}} + \eta_{\text{O}}(p_i) \times M_{\text{O}} + \eta_{\text{OH}}(p_i) \times M_{\text{OH}})/N_{\text{A}}}{\rho_{\text{silica}}} \tag{11}$$

  where the molecular weights (M) of Si, O and OH are 28.08, 16 and 17.01 kg/mol respectively. N_{A} is the Avogadro constant and the density of fused silica ρ_{silica} is 2200 kg/m^3.

- **Primary particle diameter**: $d_{\text{p}}(p_i)$ of a primary p_i is calculated by assuming each primary particle to be spherical:

$$d_{\text{p}}(p_i) = \left(\frac{6v(p_i)}{\pi}\right)^{\frac{1}{3}}. \tag{12}$$

- **Primary particle surface**: $s(p_i)$ of primary p_i is given by:

$$s(p_i) = \pi(d_{\text{p}}(p_i))^2. \tag{13}$$

- **Particle volume**: The sum of the volumes of all the primaries is equal to the volume $V(P_q)$ of the particle P_q:

$$V(P_q) = \sum_{i=1}^{n(P_q)} v(p_i). \tag{14}$$

- **Surface area of particle**: Surface area $S(P_q)$ of the particle P_q is calculated based on the average sintering level of the particle:

$$S(P_q) = \frac{S_{\text{sph}}(P_q)}{s_{\text{avg}}(1 - n(P_q)^{-\frac{1}{3}}) + n(P_q)^{-\frac{1}{3}}}, \tag{15}$$

  where $S_{\text{sph}}(P_q) = \sqrt[3]{\pi}(6V(P_q))^{\frac{2}{3}}$ is the spherical surface of P_q, $n(P_q)$ is the number of primaries and $s_{\text{avg}}(P_q)$ is the average sintering level of the particle defined as:

$$s_{\text{avg}}(P_q) = \frac{\sum_{i,j=1}^{n(P_q)} s(p_i, p_j)}{n(P_q) - 1}. \tag{16}$$

  $s(p_i, p_j)$ is the sintering level between primaries p_i and p_j (details in §2.2.2) and is defined in terms of type space variable C_{ij} by (42).

- **Collision diameter**: The collision diameter $d_{\mathrm{c}}(P_q)$ of particle P_q is calculated (as proposed by [21]) using:

$$d_{\mathrm{c}}(P_q) = d_{\mathrm{p,avg}}(P_q) n_{\mathrm{r}}(P_q)^{\frac{1}{D_{\mathrm{f}}}}. \tag{17}$$

D_{f} is the fractal dimension of the nanoparticles and is assumed to have a value of 1.8 [15]. $d_{\mathrm{p,avg}}$ is the average primary particle diameter of P_q, given by:

$$d_{\mathrm{p,avg}}(P_q) = \frac{\sum_{i=1}^{n(P_q)} d_{\mathrm{p}}(p_i)}{n(P_q)}. \tag{18}$$

$n_{\mathrm{r}}(P_q)$ is the reduced number of primary particles calculated to account for the reduction in size due to sintering events:

$$n_{\mathrm{r}}(P_q) = \frac{S(P_q)^3}{36\pi V(P_q)^2}, \tag{19}$$

$S(P_q)$ and $V(P_q)$ are calculated using (15) and (14) respectively.

- **Si:O ratio**: The total number of Si, O and OH units in a single particle can be calculated by summing the respective properties over all the primaries in the particle. Thus, at a given time,

$$\eta_x(P_q) = \sum_{i=1}^{n(P_q)} \eta_x(p_i), \tag{20}$$

where $\eta_x(P_q)$ is the number of chemical units of type x in particle P_q, $x \in \{\mathrm{Si}, \mathrm{O}, \mathrm{OH}\}$. The Si:O ratio at a given time in a single particle P_q is then given by:

$$\mathrm{Si{:}O}(P_q) = \frac{\eta_{\mathrm{Si}}(P_q)}{\eta_{\mathrm{O}}(P_q) + \eta_{\mathrm{OH}}(P_q)}. \tag{21}$$

2.2.2 Particle processes

Different particle processes are responsible for changing the state space of the particle ensemble. This subsection describes these processes, their rates and how they transform the type of the particle.

Inception: The collision of two molecules in the gas phase introduces a new particle into the system consisting of one primary. An inception event is represented in Fig. 1.

An inception event increases the number of particles in the system, $N \leftarrow N + 1$.

$$\mathrm{molecule} + \mathrm{molecule} \rightarrow P_N(p_1, \mathbf{C}) \tag{22}$$

The initial state of the constituent primary particle (p_1) is given by:

$$p_1 = p_1(\eta_{\mathrm{Si}} = 2, \eta_{\mathrm{O}} = 1, \eta_{\mathrm{OH}} = 6). \tag{23}$$

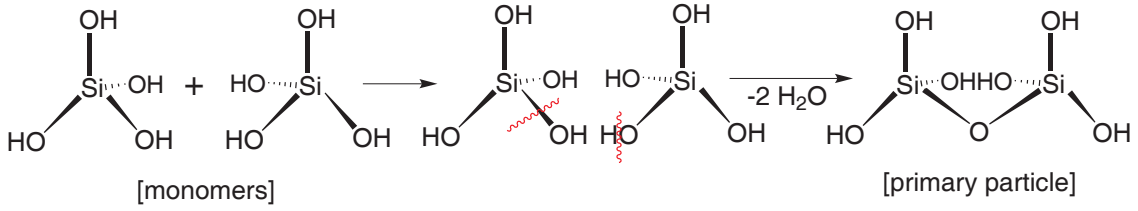

Figure 1: *Inception of primary particles from gas-phase monomers.*

The rate of inception R_{inc} is calculated for each particle (P_q) using the free molecular kernel as:

$$R_{\text{inc}}(P_q) = \frac{1}{2} K^{\text{fm}} {N_{\text{A}}}^2 C^2_{\text{Si(OH)}_4}, \tag{24}$$

$C_{\text{Si(OH)}_4}$ is the gas-phase concentration of the incepting species Si(OH)$_4$ (see §2.1) and K^{fm} is the free molecular regime coagulation kernel given by:

$$K^{\text{fm}} = 4\sqrt{\frac{\pi k_{\text{B}} T}{m_{\text{g}}}}(d_{\text{g}}^2), \tag{25}$$

where, k_{B} is the Boltzmann constant, T is the system temperature, m_{g} and d_{g} are the mass and diameter of the gas-phase molecule Si(OH)$_4$ respectively calculated from quantum chemistry calculations [18]. The gas-phase concentration of Si(OH)$_4$ is correspondingly adjusted with each inception reaction as:

$$\Delta_{\text{inc}} C_{\text{Si(OH)}_4} = -\frac{2}{N_{\text{A}} V_{\text{smpl}}}, \tag{26}$$

Each inception reaction also results in the release of one water molecule which is accounted for using the equation:

$$\Delta_{\text{inc}} C_{\text{H}_2\text{O}} = \frac{1}{N_{\text{A}} V_{\text{smpl}}}, \tag{27}$$

where $\Delta_{\text{inc}} C_{\text{Si(OH)}_4}$ and $\Delta_{\text{inc}} C_{\text{H}_2\text{O}}$ are the change in the concentration of Si(OH)$_4$ and H_2O due to inception respectively and V_{smpl} is the system sampling volume described in (72).

Surface Reaction: Surface reactions happen when one –OH group from gas phase monomer reacts with an –OH site on the particle removing one water molecule as shown in Fig. 2. In this process, one –OH site is decreased and three new –OH sites are added.

The surface reaction is the reaction of a gas-phase molecule (Si(OH)$_4$) on an –OH site on the particle P_q described by:

$$P_q + \text{molecule} \rightarrow P_q(p_1, ., p_i', .., p_{n(P_q)}, \mathbf{C}'). \tag{28}$$

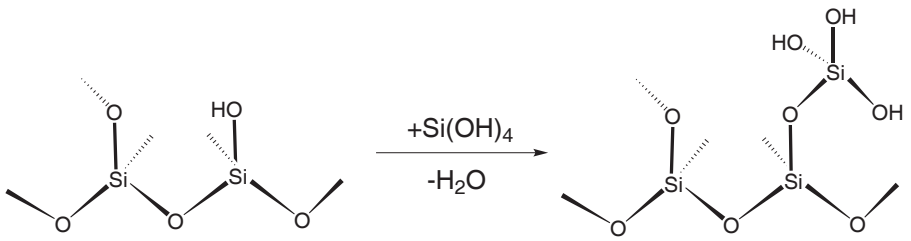

Figure 2: *Surface reaction between a particle and a gas-phase molecule.*

Primary p_i of particle P_q is uniformly selected and is tranformed as:

$$p_i \rightarrow p_i' = p_i(\eta_{\text{Si}} + 1, \eta_{\text{O}} + 1, \eta_{\text{OH}} + 2). \tag{29}$$

Rounding due to surface reaction: Surface reaction also alters the sintering matrix ($\mathbf{C} \rightarrow \mathbf{C}'$) in the following way. If a gas phase monomer reacts on the surface of a particle it changes its mass and volume. The change in volume results in the change in net common surface area of the primary particle p_i with all its neighbouring primaries. This change is given by:

$$\Delta s(p_i) = (v({p_i}') - v(p_i))\frac{2\sigma}{d_{\text{p}}(p_i)}. \tag{30}$$

σ is the surface smoothing factor such that $0 \leq \sigma \leq 2$ [21].

The corresponding change in $\mathbf{C}'$ is given by:

$$C'_{ij} = \begin{cases} 0, \text{ if } p_i \text{ and } p_j \text{ are non-neighbouring}, \\ C_{ij} + \Delta s(p_i), \text{ if } p_i \text{ and } p_j \text{ are neighbouring.} \end{cases} \tag{31}$$

Thus, for one surface reaction event on primary p_i of particle P_q, the row i and the column i of $\mathbf{C}$ are altered.

The rate of surface particle reaction (R_{surf}) for each particle (P_q) is calculated by using a reaction rate equation of Arrhenius form. The rate of *reactive* collisions takes the form:

$$R_{\text{surf}}(P_q) = A_{\text{surf}} \exp\left(-\frac{E_{\text{a}}}{RT}\right)\eta_{\text{OH}}(P_q)N_{\text{A}}C_{\text{Si(OH)}_4} \tag{32}$$

where A_{surf} is the reaction pre-exponential factor (currently set to collision-limit, *i.e.*, 1×10^{13}), E_{a} is the activation energy for a dehydration reaction between two –OH sites (currently set to 0) and T is the system temperature. $C_{\text{Si(OH)}_4}$ is the gas-phase concentration and $\eta_{\text{OH}}(P_q)$ is the total number of –OH sites on particle P_q and is give by $\sum_{i=1}^{n(P_q)} \eta_{\text{OH}}(p_i)$.

The gas-phase concentration of Si(OH)_4 is adjusted for each surface reaction as:

$$\Delta_{\text{surf}}C_{\text{Si(OH)}_4} = -\frac{1}{N_{\text{A}}V_{\text{smpl}}}, \tag{33}$$

The corresponding change in concentration of H_2O due to surface reaction is calculated as:

$$\Delta_{\text{surf}} C_{\text{H}_2\text{O}} = \frac{1}{N_{\text{A}} V_{\text{smpl}}}. \tag{34}$$

Coagulation: Coagulation occurs when two particles stick to each other and assume a point contact. The coagulation of particles P_q and P_r is implemented as follows in the model:

$$P_q(p_1, \ldots, p_{n(P_q)}, \mathbf{C}) + P_r(p_1, \ldots, p_{n(P_r)}, \mathbf{C}) \rightarrow P_s(p_1, \ldots, p_{n(P_q)}, p_{(n(P_q)+1)}, \ldots \\ \ldots, p_{n(P_q)+n(P_r)}, \mathbf{C}).$$

It is assumed that a primary particle p_i from P_q and a primary particle p_j from P_r are in point contact, *i.e.*, P_q and P_r stick to each other at the contact point of p_i and p_j. The primaries p_i and p_j are uniformly selected. The matrix $\mathbf{C}(P_s)$ is calculated accordingly as:

$$\mathbf{C}(P_s) = \begin{pmatrix} & & \vdots & \\ & \mathbf{C}(P_q) \quad \cdots \quad C_{ij} & & \cdots \\ & \vdots & \vdots & \\ \cdots & C_{ji} \quad \ldots \quad \mathbf{C}(P_r) & & \\ & \vdots & & \end{pmatrix} \tag{35}$$

where, $\mathbf{C}(P_s)$ is the connectivity matrix belonging to particle P_s with dimension $n(P_s) \times n(P_s)$, $n(P_s) = n(P_q) + n(P_r)$ and $C_{ij} = s(p_i) + s(p_j)$.

The rate of coagulation between two particles P_q and P_r is given by the transition coagulation kernel:

$$K^{\text{tr}}(P_q, P_r) = \frac{K^{\text{sf}}(P_q, P_r) K^{\text{fm}}(P_q, P_r)}{K^{\text{sf}}(P_q, P_r) + K^{\text{fm}}(P_q, P_r)}, \tag{36}$$

where the slip-flow kernel $K^{\text{sf}}(P_q, P_r)$ is given by:

$$K^{\text{sf}}(P_q, P_r) = \frac{2 k_{\text{B}} T}{3\mu} \left(\frac{1 + 1.257\text{Kn}(P_q)}{d_{\text{c}}(P_q)} + \frac{1 + 1.257\text{Kn}(P_r)}{d_{\text{c}}(P_r)} \right) (d_{\text{c}}(P_q) + d_{\text{c}}(P_r)), \tag{37}$$

where μ is the viscosity of gas-phase, d_{c} is the collision diameter of a particle and $\text{Kn}(P_q)$ and $\text{Kn}(P_r)$ are the Knudsen numbers of particles P_q and P_r, which is defined for a particle P_q as:

$$\text{Kn}(P_q) = 4.74 \times 10^{-8} \frac{T}{P d_{\text{c}}(P_q)}. \tag{38}$$

T and P are the system pressure and temperature respectively.

The free molecular collision kernel is defined by:

$$K^{\text{fm}}(P_q, P_r) = 2.2\sqrt{\frac{\pi k_{\text{B}} T}{2}}\left(\frac{1}{m(P_q)} + \frac{1}{m(P_r)}\right)^{\frac{1}{2}}\left(d_{\text{c}}(P_q) + d_{\text{c}}(P_r)\right)^2, \tag{39}$$

where $m(P_q)$ and $m(P_r)$ are masses of particles P_q and P_r respectively. Note that coagulation occurs between two particles and is thus a non-linear process.

Sintering: The sintering process is studied using the viscous-flow model in which it is assumed that the excess agglomerate surface area over that of a spherical particle with the same mass decays exponentially. A sintering step reduces the surface area of a particle as shown in **Fig. 3**.

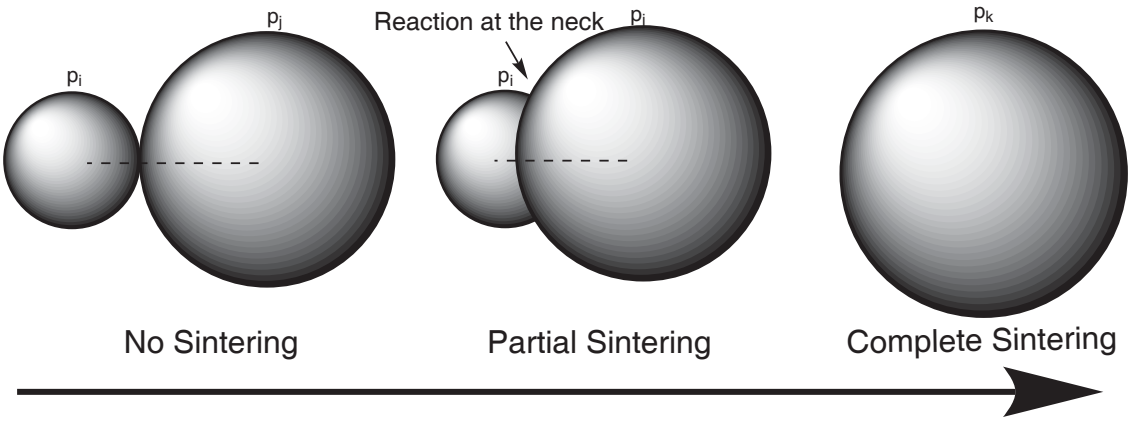

Figure 3: *Evolution of sintering process with time.*

In the current model sintering happens between two neighbouring primaries p_i and p_j of a single particle P_q. The rate of sintering between two primaries p_i and p_j is equivalent to the rate of change of their common surface ΔC_{ij} after a time interval Δt.

$$\frac{\Delta C_{ij}}{\Delta t} = -\frac{1}{\tau_{\text{s}}(p_i, p_j)}(C_{ij} - S_{\text{sph}}(p_i, p_j)), \tag{40}$$

where C_{ij} is the net common surface of primaries p_i and p_j and $S_{\text{sph}}(p_i, p_j)$ is the surface area of a sphere with the same volume as the two primaries (defined in (43)).

$\tau_{\text{s}}(p_i, p_j)$ is the characteristic sintering time of p_i and p_j and is calculated using the formula of Tsantilis et al. [26] as:

$$\tau_{\text{s}}(p_i, p_j) = A_{\text{s}} \times d_{\text{p}}(p_i, p_j) \times \exp\left(\frac{E_{\text{s}}}{T}\left(1 - \frac{d_{\text{p,crit}}}{d_{\text{p}}(p_i, p_j)}\right)\right), \tag{41}$$

where $d_{\text{p}}(p_i, p_j)$ is the minimum diameter of the two neighbouring primaries p_i and p_j. $d_{\text{p,crit}}$ is the critical diameter below which the primaries are assumed to be liquid like (*i.e.*, the sintering is instantaneous). The sintering parameters A_{s}, E_{s} and $d_{\text{p,crit}}$

are the free parameters in this model, and have been determined by fitting the model to experimental values of Seto et al. [22] in [24].

A sintering level $s(p_i, p_j)$ is defined to represent the degree of sintering between two primaries p_i and p_j as:

$$s(p_i, p_j) = \frac{\frac{S_{\text{sph}}(p_i,p_j)}{C_{ij}} - 2^{-\frac{1}{3}}}{1 - 2^{-\frac{1}{3}}}. \tag{42}$$

$S_{\text{sph}}(p_i, p_j)$ is the surface area of a sphere with the same volume as that of primaries p_i and p_j:

$$S_{\text{sph}}(p_i, p_j) = \sqrt[3]{\pi}[6\,(v(p_i) + v(p_j))]^{\frac{2}{3}} \tag{43}$$

Note that $(0 \leq s(p_i, p_j) \leq 1)$ for all primaries; for a detailed derivation refer to §A . It is assumed that two primaries p_i and p_j are completely sintered if the sintering level $s(p_i, p_j)$ is greater than 0.95. The type of particle P_q can conditionally change depending on the value of $s(p_i, p_j)$.

$$P_q(p_1, \ldots, p_{n(P_q)}, \mathbf{C}) \rightarrow \begin{cases} P_q(p_1, .., p_i', p_j', .., p_{n(P_q)}, \mathbf{C}'), \text{ if } s(p_i, p_j) < 0.95\,, \\ P_q(p_1, .., p_k'', .., p_{n(P_q)}, \mathbf{C}''), \text{ if } s(p_i, p_j) \geq 0.95. \end{cases} \tag{44}$$

- **Case 1:** $\mathbf{s(p_i, p_j) < 0.95}$**:** If the primaries p_i and p_j are not fully sintered, then their surface areas are reduced by a finite amount due to sintering. It is assumed that as the net surface of two particles decreases due to sintering and the contact surface increases, all the –OH sites at the contact surface react to form Si–O–Si bonds. The reaction between two –OH sites results in the creation of a free O unit and the removal of a water molecule as shown in Fig. 4.

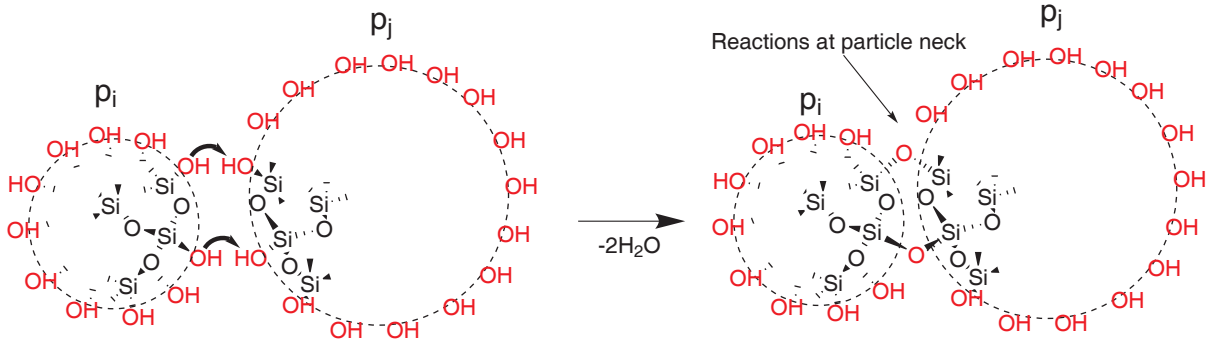

Figure 4: *Reaction due to sintering between primary particles p_i and p_j resulting in removal of two water molecules*

The surface density of active sites on a particle P_q is calculated by $\rho_{\text{s}}(P_q) = \eta_{\text{OH}}(P_q)/S(P_q)$ and is assumed to be constant throughout the process of sintering. The effect of the change of surface is thus reflected in the change of

internal variables of the primaries as given by (45), (46) and (47):

$$\Delta\eta_{\text{OH}}(p_i) = \Delta\eta_{\text{OH}}(p_j) = \lfloor \rho_{\text{s}}(P_q)\Delta C_{ij}/2 \rfloor, \tag{45}$$

Since the consumption of two OH units leads to the formation of one O unit, the change in number of O units is given by:

$$\Delta\eta_{\text{O}}(p_i) = \Delta\eta_{\text{O}}(p_j) = -\lfloor \Delta\eta_{\text{OH}}(p_i)/2 \rfloor. \tag{46}$$

The number of Si sites is invariant under the sintering process:

$$\Delta\eta_{\text{Si}}(p_i) = \Delta\eta_{\text{Si}}(p_j) = 0. \tag{47}$$

The change in type space is now given by:

$$P_q(p_1, \ldots, p_{n(P_q)}, \mathbf{C}) \rightarrow P_q(p_1, .., p_i', p_j', .., p_{n(P_q)}, \mathbf{C}'), \tag{48}$$

where

$$p_i' = p_i(\eta_{\text{Si}}, \eta_{\text{O}} - \Delta\eta_{\text{O}}(p_i), \eta_{\text{OH}} - \Delta\eta_{\text{OH}}(p_i)), \tag{49}$$

$$p_j' = p_j(\eta_{\text{Si}}, \eta_{\text{O}} - \Delta\eta_{\text{O}}(p_j), \eta_{\text{OH}} - \Delta\eta_{\text{OH}}(p_j)). \tag{50}$$

The matrix element C_{ij}' is given by:

$$C_{ij}' = C_{ij} - \frac{\Delta t}{\tau(p_i, p_j)} \left(C_{ij} - S_{\text{sph}}(p_i, p_j) \right). \tag{51}$$

- **Case 2:** $\mathbf{s(p_i, p_j) \geq 0.95}$ **:** In this case the two primary particles p_i and p_j are considered to be completely sintered. This is accounted for in the model by replacing the neighbouring primary particles p_i and p_j by a new primary p_k''. The change in type space is now given by:

$$P_q(p_1, \ldots, p_{n(P_q)}, \mathbf{C}) \rightarrow P_q(p_1, .., p_k'', .., p_{n(P_q)}, \mathbf{C}''). \tag{52}$$

The new primary p_k'' is given by:

$$p_k'' = p_k'' \left(\eta_{\text{Si}}(p_i) + \eta_{\text{Si}}(p_j), \eta_{\text{O}}(p_i) + \eta_{\text{O}}(p_j), \eta_{\text{OH}}(p_i) + \eta_{\text{OH}}(p_j) \right). \tag{53}$$

The square matrix $\mathbf{C}$ is changed by removing columns and rows i and j:

$$\left(\begin{array}{ccc|ccc|ccc} 0 & \cdots & & 0 & \cdots & & 0 & \cdots & 0 \\ \vdots & \ddots & & \vdots & & & \vdots & & \vdots \\ \hline C_{i1} & \cdots & & 0 & \cdots & & 0 & \cdots & 0 \\ \hline \vdots & \ddots & & \vdots & \ddots & & \vdots & & \vdots \\ C_{j1} & \cdots & & \cdots & \cdots & & 0 & \cdots & 0 \\ \hline \vdots & \vdots & & \vdots & \vdots & & \vdots & \ddots & \vdots \\ C_{n(P_q)1} & \cdots & & C_{n(P_q)i} & \cdots & & C_{n(P_q)j} & \cdots & 0 \end{array}\right), \tag{54}$$

followed by adding a new column and row k, to store the common surface of the new merged primary p_k and its neighbours:

$$\mathbf{C}'' = \begin{pmatrix} 0 & \cdots & 0 & \cdots & 0 \\ \vdots & \ddots & \vdots & \vdots & \vdots \\ C''_{k1} & \cdots & 0 & \cdots & 0 \\ \vdots & \vdots & \vdots & \ddots & \vdots \\ C_{(n(P_q)-1)1} & \cdots & C''_{(n(P_q)-1)k} & \cdots & 0 \end{pmatrix}. \tag{55}$$

The equations above describe sintering between only neighbouring primaries p_i and p_j, however, at every time interval (Δt), sintering is calculated between all neighbouring primaries within a particle and C_{ij} and $s(p_i, p_j)$ updated.

Sintering results in the release of water molecules as shown in Fig. 4. The reaction of two –OH groups results in the formation of one H_2O molecule. The gas-phase concentration of water is therefore adjusted after sintering as:

$$\Delta_{\text{sint}} C_{\text{H}_2\text{O}} = -\frac{\sum_{q=1}^{N} \Delta_{\text{sint}} \eta_{\text{OH}}(P_q)/2}{N_{\text{A}} V_{\text{smpl}}}, \tag{56}$$

where $\Delta_{\text{sint}} \eta_{\text{OH}}(P_q) = \sum_{i=1}^{n(P_q)} \Delta \eta_{\text{OH}}(p_i)$ is the change in the number of –OH units in particle P_q resulting from sintering.

Intra-particle reaction: This process results in the reduction of –OH units in the particle. To attain a stoichiometric ratio of Si:O of 1:2, the number of –OH sites in the particles should be minimised to zero. A typical one step intra-particle reaction is given in Fig. 5.

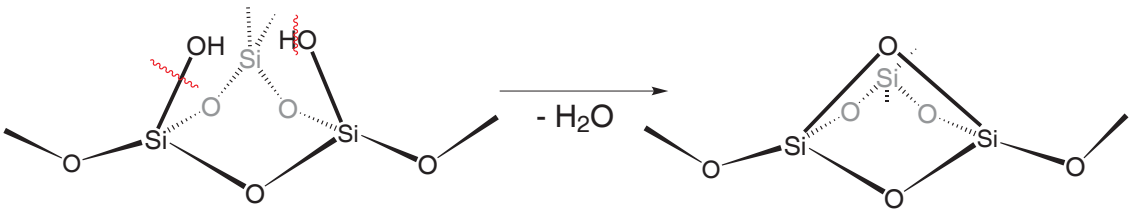

Figure 5: *Intra-particle reaction.*

A single intra-particle reaction alters the type space of particle P_q as:

$$P_q(p_1, .., p_i, .., p_{n(P_q)}, \mathbf{C}) \rightarrow P_q(p_1, .., p'_i, .., p_{n(P_q)}, \mathbf{C}). \tag{57}$$

A primary particle p_i of particle P_q is uniformly selected and transformed as:

$$p_i \rightarrow p'_i = p_i(\eta_{\text{Si}}, \eta_{\text{O}} + 1, \eta_{\text{OH}} - 2). \tag{58}$$

$\mathbf{C}$ is assumed to be constant during an intra-particle reaction. It is assumed that the removal of one water molecule does not alter the mass (and hence diameter) of

the primary by a large amount, and thus its common surface with other primaries remains unchanged.

The rate of intra-particle reaction is calculated for each particle P_q such that the Si:O ratio in the particle is always 1:2. This gives:

$$R_{\text{int}}(P_q) = A_{\text{surf}} \exp\left(-\frac{E_{\text{a}}}{RT}\right) \eta_{\text{OH}}(P_q) N_{\text{A}} C_{\text{Si(OH)}_4} - \frac{\rho_{\text{s}}(P_q)}{2} \left[\sum_{i,j=1}^{n(P_q)} \frac{C_{ij} - S_{\text{sph}}(p_i, p_j)}{\tau(p_i, p_j)}\right], \tag{59}$$

where, $\eta_{\text{OH}}(P_q)$ is the number of OH units in particle P_q, $\rho_{\text{s}}(P_q) = \eta_{\text{OH}}(P_q)/S(P_q)$ is the surface density of active sites. A_{surf} and E_{a} are rate parameters of surface reaction defined in §2.2.2, N_{A} and $C_{\text{Si(OH)}_4}$ are the Avogadro constant and the gas-phase concentration of Si(OH)_4 respectively. C_{ij} is the net common surface area of primaries p_i and p_j (§2.2.2). For a detailed derivation of (59), refer to §A.

The change in the gas-phase concentration of water due to an intra-particle reaction event is given by:

$$\Delta_{\text{int}} C_{\text{H}_2\text{O}} = \frac{1}{N_{\text{A}} V_{\text{smpl}}}. \tag{60}$$

2.3 Algorithm

2.3.1 Operator Splitting

From (24), (32) and (59), it is apparent that the rates of certain particle processes depend on the concentration of the gas-phase precursor Si(OH)_4. The particle processes, in turn, lead to the alteration of the gas-phase by consuming Si(OH)_4 ((26) and (33)) and by releasing H_2O ((27), (34), (56) and (60)). The gas-phase chemistry and the particle processes are thus inherently coupled. In order to realise this coupling, an *Operator-Splitting technique*, developed by Celnik et al. [2] is used.

The state of the system (Q) at any time consists of two components.

1. The first component (Q_1) contains the concentration of the chemical species:

$$Q_1 = \{C_k : k \in \{1, \ldots, N_{\text{g}}\}\}, \tag{61}$$

where C_k is the gas-phase concentration of the k^{th} species and N_{g} is the number of gas-phase species.

2. The second component (Q_2) is the stochastic particle system:

$$Q_2 = \{P_q : q \in \{1, \ldots, N\}\}, \tag{62}$$

where P_q is the q^{th} particle in the system (7) and N is the total number of particles in the system.

The operator $\mathcal{G}$ represents the effects of gas-phase chemical reactions on the system and the operator $\mathcal{P}$ indicates the effects of the particle processes on the system. This is written as:

$$\frac{\mathrm{d}}{\mathrm{d}t}\begin{pmatrix} Q_1 \\ Q_2 \end{pmatrix} = \begin{pmatrix} \mathcal{G}_1\left(Q_1\right) \\ \mathcal{G}_2\left(Q_1, Q_2\right) \end{pmatrix} + \begin{pmatrix} \mathcal{P}_1\left(Q_1, Q_2\right) \\ \mathcal{P}_2\left(Q_1, Q_2\right) \end{pmatrix}, \tag{63}$$

where subscripts 1 and 2 denote gas-phase and particle-phase respectively.

- $\mathcal{G}_1$ is the gas-phase operator operating on the gas-phase chemical mechanism and is given by:

$$\mathcal{G}_1(C_k) = \dot{m}_k(C_k, T) - \gamma(C_k, T)C_k, \tag{64}$$

  where C_k and $\dot{m}_k$ are the gas-phase concentration and the molar production rate of the k^{th} species. T is the temperature of the system and γ is the rate of gas-phase expansion calculated in (6).

- $\mathcal{G}_2$ indicates the change to the particle ensemble due to gas-phase processes. For a constant pressure system this describes the expansion of gas and hence a decrease in particle number density.

$$\mathcal{G}_2(Q_1, Q_2) = -\gamma(C_k, T)Q_2 \tag{65}$$

- $\mathcal{P}_1$ is the change to the gas-phase chemistry due to particle processes:

$$\mathcal{P}_1(Q_1, Q_2) = \dot{g}_k(Q_1, Q_2), \tag{66}$$

  where $\dot{g}_k$ is the molar rate of production of species k due to particle processes. In the current work, the particle processes alter the gas-phase concentrations of two chemical species, namely, $\mathrm{Si(OH)_4}$ and $\mathrm{H_2O}$. The rates of production of these two species are calculated as follows.

  In a time interval Δt, let the number of inception, surface reaction and intra-particle reactions in the ensemble are given by N_{inc}, N_{surf} and N_{int} respectively. Using (26) and (33), the molar rate of production of $\mathrm{Si(OH)_4}$ is given by:

$$\dot{g}_{\mathrm{Si(OH)_4}} = -\frac{2N_{\text{inc}} + N_{\text{surf}}}{N_{\text{A}} V_{\text{smpl}} \Delta t}. \tag{67}$$

  Correspondingly, the molar rate of production of $\mathrm{H_2O}$ is calculated using (27), (34), (56) and (60).

$$\dot{g}_{\mathrm{H_2O}} = \frac{N_{\text{inc}} + N_{\text{surf}} + N_{\text{int}} - \sum_{q=1}^{N} \Delta_{\text{sint}}\eta_{\text{OH}}(P_q)/2}{N_{\text{A}} V_{\text{smpl}} \Delta t}. \tag{68}$$

  Here, $\Delta_{\text{sint}}\eta_{\text{OH}}(P_q)$ is the change in the number of –OH units in particle P_q in time Δt due to sintering.

- $\mathcal{P}_2$ is the change to the particle ensemble due to particle processes and is given by:

$$\mathcal{P}_2(Q_1, Q_2) = \mathcal{I}(Q_1, Q_2) + \mathcal{K}(Q_2) + \mathcal{S}(Q_1, Q_2) + \mathcal{Z}(Q_1, Q_2) + \mathcal{X}(Q_1, Q_2), \quad (69)$$

  where $\mathcal{I}$, $\mathcal{K}$, $\mathcal{S}$, $\mathcal{Z}$ and $\mathcal{X}$ are the inception, coagulation, surface reaction, sintering and intra-particle reaction operators respectively, details of which are given in §2.2.2.

The gas-phase chemistry is solved using an ODE solver and the population balance equations are solved using **Algorithm 2**. The batch reactor system considered in this work is an initial value problem and a forward time stepping algorithm is used. The solution at time t_i is given by $(Q_{1,i}, Q_{2,i})$. Using an operator splitting over this time step, it can be solved in two stages: first using the ODE solver and then using the population balance solver. In the current work, splitting is further refined using the method of Strang [25].

The algorithm for performing the operator splitting is described in **Algorithm 1**.

Input: State of the system $Q_0 = Q_{1,0} + Q_{2,0}$ at initial time t_0; Final time t_f.
Output: State of the system Q_f at final time t_f.
$t_i \longleftarrow t_0$, $Q_i \longleftarrow Q_0$;
while $t_i < t_\mathrm{f}$ **do**

Integrate over time interval $[t_i, t_i + \frac{h}{2}]$ (using an ODE solver)

$$\frac{\mathrm{d}}{\mathrm{d}t}\begin{pmatrix} Q_1^1 \\ Q_2^1 \end{pmatrix} = \begin{pmatrix} \mathcal{G}_1\left(Q_1^1\right) \\ \mathcal{G}_2\left(Q_1^1, Q_2^1\right) \end{pmatrix}$$

with initial conditions

$$\begin{pmatrix} Q_1^1(t_i) \\ Q_2^1(t_i) \end{pmatrix} = \begin{pmatrix} Q_{1,i} \\ Q_{2,i} \end{pmatrix}.$$

Solve (using **Algorithm 2**) over time interval $[t_i, t_i + h]$

$$\frac{\mathrm{d}}{\mathrm{d}t}\begin{pmatrix} Q_1^2 \\ Q_2^2 \end{pmatrix} = \begin{pmatrix} \mathcal{P}_1\left(Q_1^2, Q_2^2\right) \\ \mathcal{P}_2\left(Q_1^2, Q_2^2\right) \end{pmatrix}$$

with initial conditions

$$\begin{pmatrix} Q_1^2(t_i) \\ Q_2^2(t_i) \end{pmatrix} = \begin{pmatrix} Q_1^1(t_i + \frac{h}{2}) \\ Q_2^1(t_i + \frac{h}{2}) \end{pmatrix}$$

Integrate over time interval $[t_i + \frac{h}{2}, t_i + h]$ (using an ODE solver)

$$\frac{\mathrm{d}}{\mathrm{d}t}\begin{pmatrix} Q_1^3 \\ Q_2^3 \end{pmatrix} = \begin{pmatrix} \mathcal{G}_1\left(Q_1^3\right) \\ \mathcal{G}_2\left(Q_1^3, Q_2^3\right) \end{pmatrix}$$

with initial conditions

$$\begin{pmatrix} Q_1^3(t_i) \\ Q_2^3(t_i) \end{pmatrix} = \begin{pmatrix} Q_1^2(t_i + h) \\ Q_2^2(t_i + h) \end{pmatrix}$$

Assign solution at $t_{i+1} = t_i + h$

$$\begin{pmatrix} Q_{1,i+1} \\ Q_{2,i+1} \end{pmatrix} \leftarrow \begin{pmatrix} Q_1^3(t_i + h) \\ Q_2^3(t_i + h) \end{pmatrix}$$

$i \longleftarrow i + 1$;

Algorithm 1: The Operator Splitting algorithm.

2.3.2 Particle doubling and contraction

The population balance solver developed in this work uses a variable size particle ensemble leading to two problematic situations: first, attempting to add a particle when there is insufficient space and second, removing particles until no particles remain. A contraction algorithm is used to solve the first problem whereby, once the ensemble capacity is saturated, a particle is uniformly selected from the ensemble and discarded. The ensemble scaling factor is updated accordingly. The second problem is corrected using a particle doubling algorithm [20]. Once the particle count reaches half of the maximum, the par-

ticles are copied and the sample volume is doubled in order to allow the maintenance of a statistically significant number of particles in the system and avoid gelation of particles into a few big particles. The maximum number of stochastic particles in the system is defined (N_{sp}) and the actual particle count lies in the range of $[\frac{1}{2}N_{\text{sp}}, N_{\text{sp}}]$ except at early times. The time profile of the ensemble particle count for $N_{\text{sp}} = 131072$ and $L = 1$ is given in **Figure 6**. The spikes in the plot are indicative of the doubling algorithm.

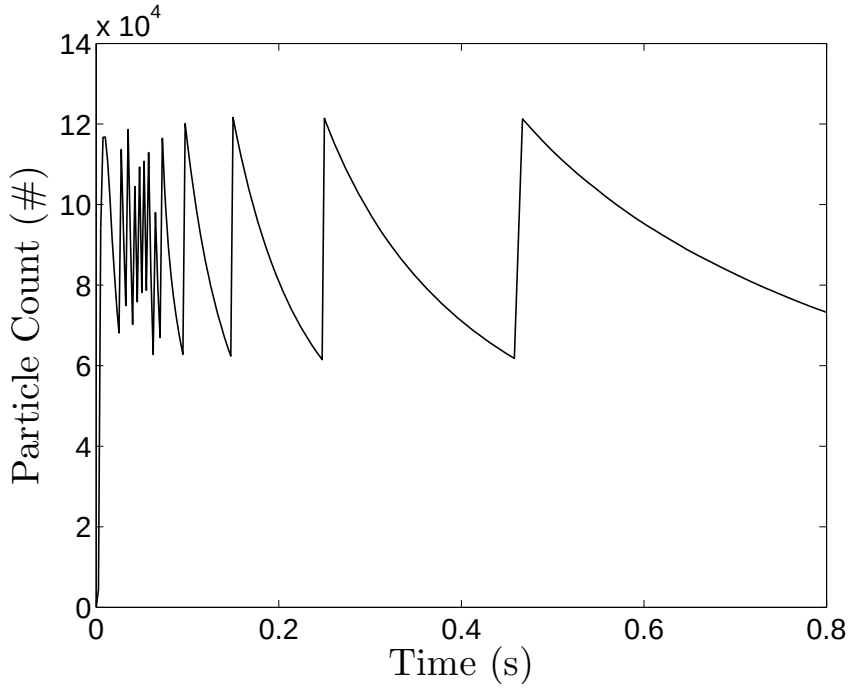

Figure 6: *Time profile of the ensemble particle count for $N_{sp} = 131072$ and $L = 1$. The spikes in the plot are indicative of the particle doubling algorithm.*

2.3.3 Direct Simulation Monte Carlo algorithm

The current work uses a Monte Carlo algorithm to solve the particle population balance equations described in §2.2.2, but with various enhancements to improve efficiency. **Algorithm 2** describes the direct simulation Monte Carlo algorithm (DSMC) used in the current work. The computation speed for performing coagulation processes is enhanced by using the technique of fictitious jumps by introducing an appropriate majorant kernel as proposed by Eibeck and Wagner [5]. The choice of the majorant kernel used for the current work has been discussed in detail by Patterson et al. [17].

Input: Initial state of the system Q_0 at time t_0; Final time t_f.
Output: State of the system Q_f at final time t_f.
$t \longleftarrow t_0$, $Q \longleftarrow Q_0$;
while $t < t_\mathrm{f}$ **do**
  Calculate an exponentially distributed waiting time τ with parameter $R_{\text{tot}}(Q)$:

$$R_{\text{tot}}(Q) = R_{\text{inc}}(Q) + R_{\text{coag}}(Q) + R_{\text{surf}}(Q) + R_{\text{int}}(Q)$$

  where $R_{\text{inc}}(Q)$, $R_{\text{coag}}(Q)$, $R_{\text{surf}}(Q)$ and $R_{\text{int}}(Q)$ are given by (24), (36), (32) and (59) respectively.
  Choose a process m with probability

$$P(m) = \frac{R_m(Q)}{R_{\text{tot}}(Q)}$$

  where R_m is the rate of the process m, with $m \in \{\text{inc}, \text{coag}, \text{surf}, \text{int}\}$.
  if $m = \text{inc}$ **then**
    Perform inception by adding a new particle P_N to the ensemble:

$$P_N(p_1(\eta_{\text{Si}} = 2, \eta_{\text{O}} = 1, \eta_{\text{OH}} = 6), \mathbf{C}).$$

    Update $C_{\text{Si(OH)}_4}$ and $C_{\text{H}_2\text{O}}$ using (26) and (27).
    if $N > N_{\text{sp}}$ **then**
      Uniformly select and remove a particle from the ensemble.
  else if $m = \text{coag}$ **then**
    Uniformly select two particles P_q and P_r.
    With a probability $K^{\text{tr}}(P_q, P_r)/\hat{K}(P_q, P_r)$ perform coagulation as:

$$P_q + P_r \rightarrow P_s(p_1, ..., p_{n(P_q)}, p_{(n(P_q)+1)}, ..., p_{n(P_q)+n(P_r)}, \mathbf{C}).$$

    where $\hat{K}(P_q, P_r) = K^{\text{fm}}(P_q, P_r)$ is the majorant kernel; $K^{\text{fm}}(P_q, P_r)$ is the free-molecular kernel (39) and $K^{\text{tr}}(P_q, P_r)$ is the transition kernel (36).
    if $N < (0.5 \times N_{\text{sp}})$ **then**
      Double the ensemble and adjust sampling volume.
  else if $m = \text{surf}$ **then**
    Uniformly select a particle P_q.
    Perform surface reaction on a uniformly selected primary p_i of the particle as:

$$P_q \rightarrow P_q(p_1, ., p_i(\eta_{\text{Si}} + 1, \eta_{\text{O}} + 1, \eta_{\text{OH}} + 2), .., p_{n(P_q)}, \mathbf{C}').$$

    Update $C_{\text{Si(OH)}_4}$ and $C_{\text{H}_2\text{O}}$ using (33) and (34).
  else
    Uniformly select a particle P_q.
    Perform intra-particle reaction on a uniformly selected primary p_i of the particle as:

$$P_q \rightarrow P_q(p_1, .., p_i(\eta_{\text{Si}}, \eta_{\text{O}} + 1, \eta_{\text{OH}} - 2), .., p_{n(P_q)}, \mathbf{C}).$$

    Update $C_{\text{H}_2\text{O}}$ using (60).
  Update sintering level of all particles using (40).
  Update $C_{\text{H}_2\text{O}}$ using (56).
  Increment $t \longleftarrow t + \tau$.

Algorithm 2: The Direct Simulation Monte Carlo algorithm.

3 Numerical studies

In this section, we present a detailed numerical study of the model described in §2. The state of the stochastic particle system Q_2 at time t is described by:

$$Q_2(t) = \left(x_1(t), \ldots, x_{N(t)}(t)\right), \tag{70}$$

where $N(t)$ is the number of computational particles in the system and each x_i is a random process. For an equally weighted particle system, there is a constant scaling between computational particles in the ensemble $N(t)$ and real particles in the physical system. The particle number density $f(t,x)$ is approximated as a sum of discrete measures:

$$f(t,x)\mathrm{d}x \sim \frac{1}{V_{\text{smpl}}} \sum_{j=1}^{N(t)} \delta_{x_j(t)}(\mathrm{d}x), \tag{71}$$

where the normalisation parameter V_{smpl} is the sampling volume which is chosen to ensure that the maximum possible number of stochastic particles lie within the sampling space:

$$V_{\text{smpl}} = \frac{N_{\text{sp}}}{M_0^{\text{max}}}, \tag{72}$$

where N_{sp} is the numerical parameter that bounds the number of computational particles in the system and M_0^{max} is a user-defined quantity which is set to the maximum particle number density expected to occur in the simulation. It is important to choose the value of the parameter M_0^{max} carefully in order to ensure that the number of particle doublings and contractions is minimal, giving statistically meaningful results with minimal computational cost.

3.1 Numerical parameters

The numerical convergence of the algorithm was investigated by solving a test system with different numerical parameters such as:

(i) Numerical parameter that determines the number of computational particles in the system (N_{sp});

(ii) Number of runs (L);

(iii) Splitting time-step (Δt_{s}).

The test system is described below. In this section, we study the convergence of a number of macroscopic properties with respect to N_{sp} in detail (keeping $N_{\text{sp}} \times L$ constant). We also investigate briefly, the convergence behaviour of certain important functionals with respect to the splitting time step (Δt_{s}).

Test Case

A simple test case was created in order to perform the numerical convergence studies. A zero-dimensional batch reactor was simulated with 250 ppm of the initial precursor (TEOS) in an inert gas (N_2). The temperature was assumed to be constant at $900\,^{\circ}\mathrm{C}$ and the pressure was set to 1 atm. No particles were present in the reactor initially. The reactor residence time t_f was 0.8 s.

3.2 Error calculations

Typical macroscopic quantities of the system such as moments, collision diameter *etc.* are of the form

$$F(t) = \int_0^\infty \varphi(x) f(t,x) \mathrm{d}x,$$

which are approximated (as $N_\mathrm{sp} \to \infty$) by the random variable

$$\xi^{N_\mathrm{sp}}(t) = \frac{1}{V_\mathrm{smpl}} \sum_{i=1}^{N(t)} \varphi(x_i(t)). \tag{73}$$

In order to estimate the expectation and fluctuation of (73), we generate a number L of independent ensembles of particles, with corresponding random variables $\xi^{(N_\mathrm{sp},1)}(t), \ldots, \xi^{(N_\mathrm{sp},L)}(t)$.

The empirical mean at time t is given by:

$$\mu_1^{(N_\mathrm{sp},L)}(t) = \frac{1}{L} \sum_{l=1}^{L} \xi^{(N_\mathrm{sp},l)}(t). \tag{74}$$

The variance $\left(\mathrm{Var}\left(\xi^{(N_\mathrm{sp},L)}(t)\right)\right)$ is given by:

$$\mu_2^{(N_\mathrm{sp},L)}(t) = \frac{1}{L} \sum_{l=1}^{L} \xi^{(N_\mathrm{sp},l)}(t)^2 - \mu_1^{(N_\mathrm{sp},L)}(t)^2. \tag{75}$$

Here, $\xi^{(N_\mathrm{sp},l)}(t)$, $\mu_1^{(N_\mathrm{sp},l)}(t)$ and $\mu_2^{(N_\mathrm{sp},l)}(t)$ denote the values of the property, its empirical mean and its empirical variance at time t for N_sp computational particles during run number l.

The confidence interval for $\mu_1^{(N_\mathrm{sp},L)}(t)$ is calculated using the central limit theorem:

$$c_P = a_P \sqrt{\frac{\mu_2^{(N_\mathrm{sp},L)}(t)}{L}}. \tag{76}$$

This gives a probabilistic upper bound for the statistical error. The value of a_P is obtained from standard normal distribution tables. In our case, we choose a 99.9% confidence inter-

val, for which $a_P = 3.29$. The confidence interval I_P within which there is a probability P of finding the true solution is then given by:

$$I_P = \left[\mu_1^{(N_{\text{sp}},L)}(t) - c_P, \mu_1^{(N_{\text{sp}},L)}(t) + c_P\right]. \tag{77}$$

The error e is then estimated as:

$$e^{(N_{\text{sp}},L)}(t) = \left|\mu_1^{(N_{\text{sp}},L)}(t) - \zeta(t)\right|, \tag{78}$$

where, $\zeta(t)$ is an approximation for the true solution which is obtained from a "high-precision calculation" with a very large number of particles, in our case $N = 131072$ (2^{17}) and $L = 10$. The average error is computed over the entire residence time as:

$$\bar{e}(N_{\text{sp}}, L) = \frac{1}{M}\sum_{j=1}^{M} e^{(N_{\text{sp}},L)}(t_j), \tag{79}$$

where the M time steps t_j are equidistant.

Correspondingly, the relative error e_{r} is calculated using:

$$e_{\text{r}}^{(N_{\text{sp}},L)}(t) = \frac{\left|\mu_1^{(N_{\text{sp}},L)}(t) - \zeta(t)\right|}{\zeta(t)}. \tag{80}$$

This quantity is averaged over the entire residence time to give the average relative error as:

$$\bar{e}_{\text{r}}(N_{\text{sp}}, L) = \frac{1}{M}\sum_{j=1}^{M} e_{\text{r}}^{(N_{\text{sp}},L)}(t_j). \tag{81}$$

The error in a quantity ξ calculated at time t using a splitting time step Δt_{s} (keeping N_{sp} and L constant) is given by:

$$e_s{}^{\Delta t_{\text{s}}}(t) = \left|\xi^{\Delta t_{\text{s}}}(t) - \zeta'(t)\right|, \tag{82}$$

where $\zeta'(t)$ is a "high-precision solution" calculated with a small value of $\Delta t_{\text{s}} = 2.5\ \mu s$. The average error computed over the entire residence time is:

$$\bar{e}_s{}^{\Delta t_{\text{s}}}(t) = \frac{1}{M}\sum_{j=1}^{M} e_s{}^{\Delta t_{\text{s}}}(t_j), \tag{83}$$

where the M time steps t_j are equidistant.

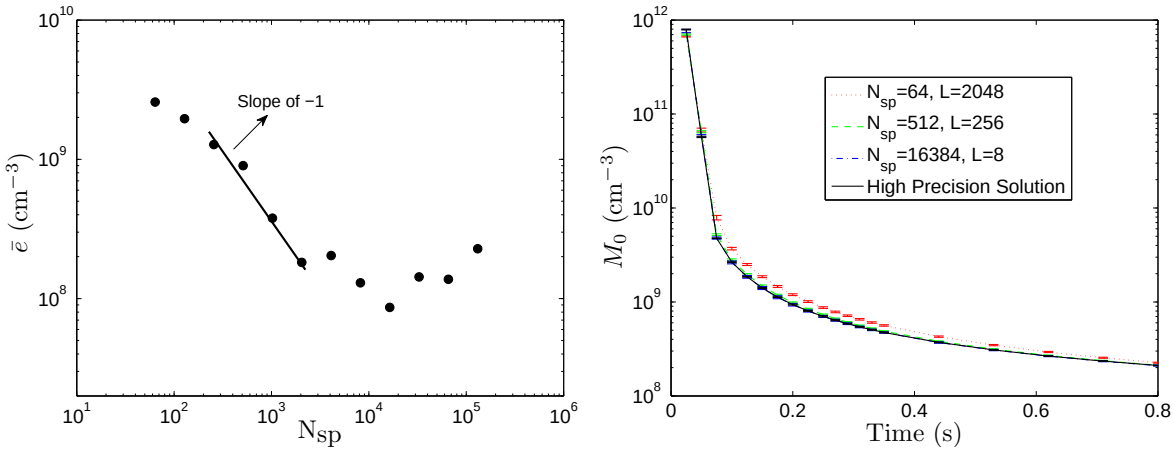

(a) *Error in M_0 as a function of N_{sp}. Solid line indicates a slope of -1.* **(b)** *Time profile of M_0 with 99.9% confidence intervals.*

Figure 7: *Convergence of the zeroth moment ($N_{\text{sp}} \times L = 131072$).*

3.3 Numerical Results

3.3.1 Convergence with respect to N_{sp}

In this section, we analyse the convergence behaviour of three key functionals: the zeroth moment M_0, the ensemble volume fraction F_{v} and the collision diameter D_{c}. Additionally, the level of detail provided by this model enables us to study a number of previously intractable properties.

Using (71), various properties of the particle ensemble can be calculated. The convergence studies reported in this section are performed by varying the values of N_{sp} and L whilst keeping their product constant at 131072 (2^{17}). The splitting time step Δt_{s} is held at a constant value of 25 μs, which was determined to be sufficiently small to obtain a reasonably converged solution (*i.e.*, halving the splitting time step has no significant impact on the error. See §3.3.4).

Zeroth moment : The zeroth moment (M_0) of the system is the particle number density:

$$M_0(t) = \frac{N(t)}{V_{\text{smpl}}}, \tag{84}$$

where $N(t)$ is the number of computational particles in the system and V_{smpl} is the sampling volume. The particle number density is altered by the creation of new particles in the system (by inception) or by the removal of particles from the system (by coagulation). The average error in M_0 calculated using (81) is presented in **Fig. 7a**. The solid line indicates a slope of -1. The time profiles of M_0 for different values of N_{sp} and L are shown in **Fig. 7b**.

Volume-fraction (F_{v}) : The average volume-fraction of the particle ensemble (*i.e.*, the fraction of the control volume occupied by the particle phase) gives the first moment

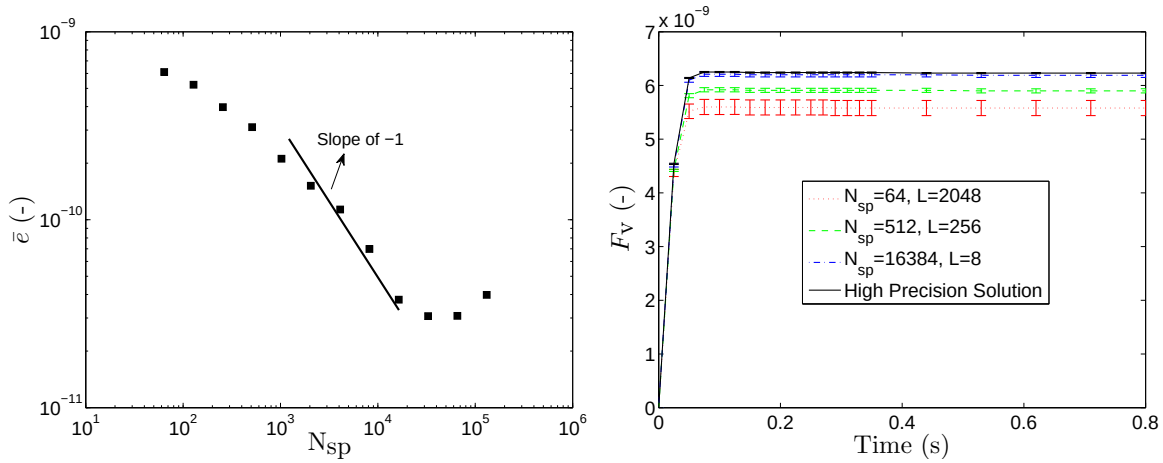

(a) *Error in F_v as a function of N_{sp}. Solid line indicates a slope of -1.* **(b)** *Time profile of F_v with 99.9% confidence intervals.*

Figure 8: *Convergence of volume-fraction ($N_{\mathrm{sp}} \times L = 131072$).*

of the ensemble. This is calculated using:

$$F_{\mathrm{v}}(t) = \frac{1}{V_{\mathrm{smpl}}} \sum_{q=1}^{N(t)} V(P_q(t)), \tag{85}$$

where $V(P_q)$ is the volume of particle P_q calculated from its chemical composition using (14), $N(t)$ is the number of particles in the system and V_{smpl} is the sampling volume. **Fig. 8a** depicts the average error in F_{v} calculated using (81). In **Fig. 8b**, the time profile of F_{v} for different values of N_{sp} and L indicates that the particle volume fraction increases for the first 0.1 s in the reactor and then stays constant. This highlights the fast conversion of gas-phase species into particle-phase which is attained in the first 0.1 s. The concentration of gas-phase species is discussed in more detail in §3.3.2.

Average Collision Diameter (D_{c}) : The average collision diameter of the particle ensemble is calculated using:

$$D_{\mathrm{c}}(t) = \frac{1}{N(t)} \sum_{q=1}^{N(t)} d_{\mathrm{c}}(P_q(t)) \tag{86}$$

where $d_{\mathrm{c}}(P_q)$ is the collision diameter of particle P_q calculated using (17). This property is often of importance for many size-sensitive industrial applications such as catalysis, support material and biomedical applications [24]. **Fig. 9a** and **Fig. 9b** depict the average error in $D_{\mathrm{c}}(t)$ (calculated using (81)) at different values of N_{sp} and the time profile of $D_{\mathrm{c}}(t)$ for different values of N_{sp} and L respectively. The average collision diameter is seen to increase with time indicating higher degrees of aggregation.

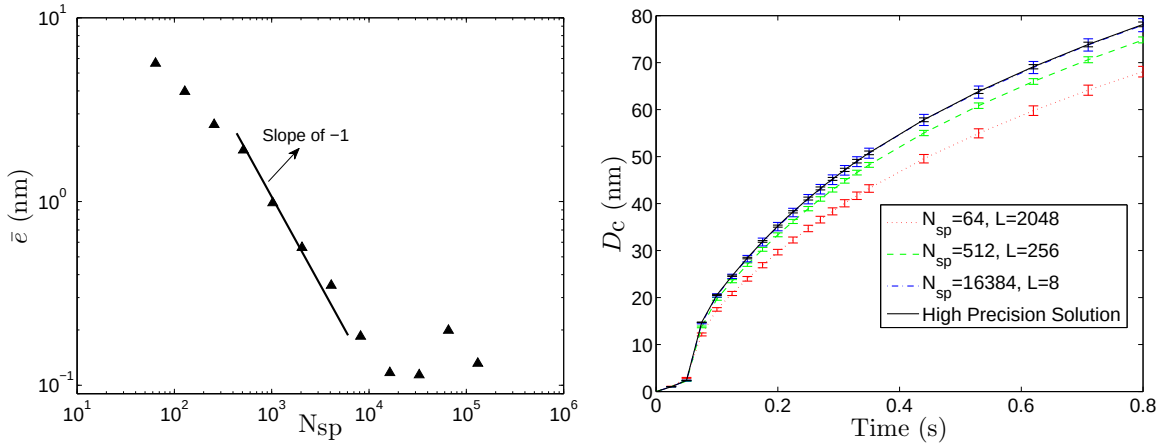

(a) *Error in D_c as a function of N_{sp}. Solid line indicates a slope of -1.* **(b)** *Time profile of D_c with 99.9% confidence intervals.*

Figure 9: *Convergence of average collision diameter ($N_{sp} \times L = 131072$).*

Other Functionals: In order to understand the complicated model developed in this work, it is useful to study the numerical behaviour of many functionals. **Table 1** lists the details of various functionals whose numerical behaviours have been observed. **Figs. 10a-13a** report the averaged values of these functionals in the ensemble at final time $t_f = 0.8$ s at different values of N_{sp}. Correspondingly, the time evolution of these quantities with 99.9% confidence interval for the reactor residence time of 0.8 s are depicted in **Figs. 10b-13b**.

It is evident from Fig. 13b that the level of sintering exhibits a monotone decreasing trend after about 0.1 s. This can be attributed to the fact that, with time, the particles become more aggregated (as confirmed by the increasing collision diameter and average number of primaries per particle in Figs. 9b and 10b respectively) which leads to a reduction in the average sintering level of the ensemble.

The averaged values of all functionals are observed to converge to a stable value as the numerical parameter N_{sp} in the simulation is increased. It is also observed that different properties show varied rates of convergence. The relative convergence speeds of different functionals is further discussed in §3.3.3.

The complexity of the type space in the current model enables us to track functionals conditioned on the basis of certain values of other functionals. In **Fig. 14a**, the particle ensemble is divided into three size classes based on the collision diameter (d_c) of the particle as: small ($d_c \in (0, 50)$ nm), medium ($d_c \in [50, 200)$ nm) and large ($d_c \geq 200$ nm) particles, and the relative error at final time $e_r(t_f)$ in sintering level for different values of the numerical parameter N_{sp} is plotted for each of these size classes. Similarly, in **Fig. 14b** the particle ensemble is divided into three different size classes based on the number of primaries per particle and the relative error at final time $e_r(t_f)$ in the stoichiometric ratio of Si:O calculated for different values of N_{sp}. The fraction of particles that are present in each size class (f_N) is also depicted. It is hypothesised that the difference in error for different classes arises due to the number of particles present in each size class.

Table 1: *Study of convergence behaviour of various functionals. Note that $N(t)$ is the number of computational particles in the ensemble at time t.*

Functional (Averaged value)	Formula	Reference figures
Primaries per particle	$\bar{n}(t) = \frac{1}{N(t)} \sum_{q=1}^{N(t)} n(P_q(t))$ $n(P_q)$: Number of primaries in particle P_q (7)	10a, 10b
Primary particle diameter	$\bar{d}_{\mathrm{p}}(t) = \frac{1}{N(t)} \sum_{q=1}^{N(t)} d_{\mathrm{p,avg}}(P_q(t))$ $d_{\mathrm{p,avg}}(P_q)$: Primary diameter of particle P_q (18)	11a, 11b
Si:O stoichiometric ratio	$\overline{\mathrm{Si{:}O}}(t) = \frac{1}{N(t)} \sum_{q=1}^{N(t)} \mathrm{Si{:}O}(P_q(t))$ $\mathrm{Si{:}O}(P_q)$: Si:O ratio of particle P_q (21)	12a, 12b
Sintering level	$\bar{s}(t) = \frac{1}{N(t)} \sum_{q=1}^{N(t)} s_{\mathrm{avg}}(P_q(t))$ $s_{\mathrm{avg}}(P_q)$: Sintering level of particle P_q (16)	13a, 13b

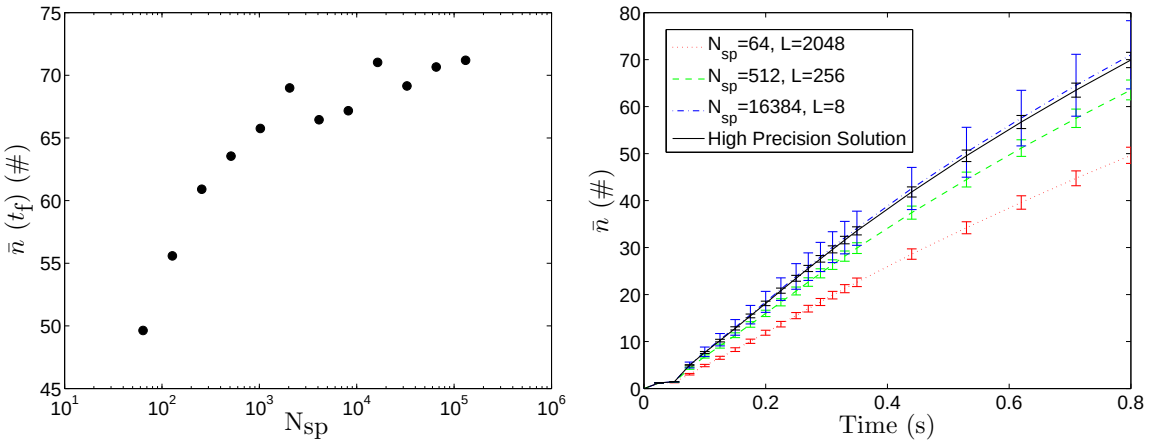

(a) *Average number of primaries per particle in the ensemble at final time.*

(b) *Time evolution of $\bar{n}$ (see Table 1) with 99.9% confidence intervals.*

Figure 10: *Convergence behaviour of average number of primaries per particle in the ensemble for different values of N_{sp}.*

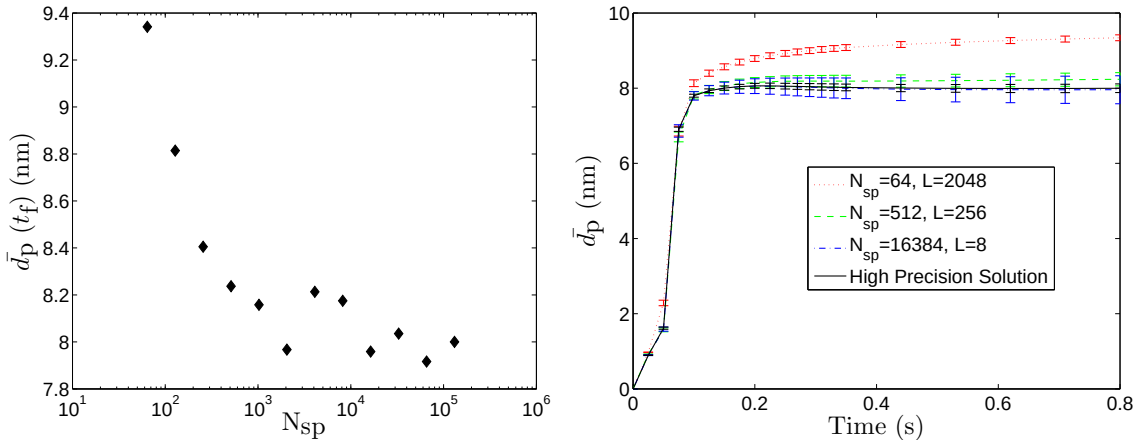

(a) *Average primary particle diameter of the ensemble at final time.* **(b)** *Time evolution of $\bar{d}_p$ (see Table 1) with 99.9% confidence intervals.*

Figure 11: *Convergence behaviour of average primary particle diameter of the ensemble for different values of N_{sp}.*

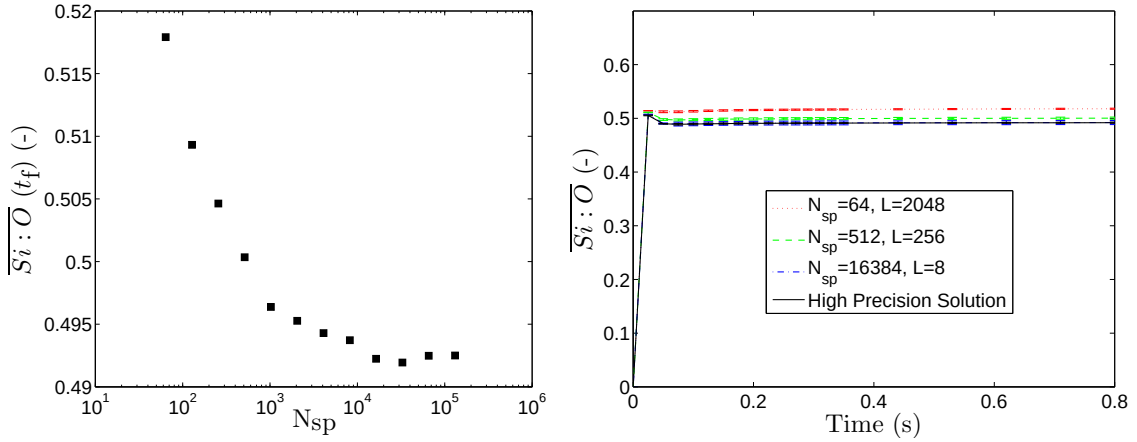

(a) *Average Si:O ratio of the ensemble at final time.* **(b)** *Time evolution of average Si:O ratio with 99.9% confidence intervals.*

Figure 12: *Convergence behaviour of average stoichiometric Si:O ratio of the ensemble for different values of N_{sp}.*

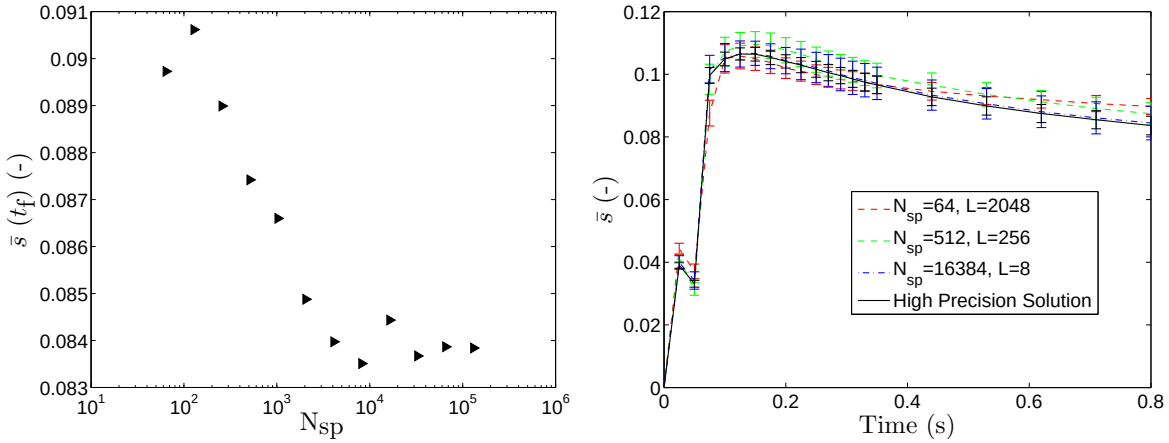

(a) *Average sintering level of the ensemble at final time.* **(b)** *Time evolution of average sintering level with 99.9% confidence intervals.*

Figure 13: *Convergence behaviour of average sintering level of the ensemble for different values of N_{sp}.*

3.3.2 Rates and jump events

As discussed in §2.2.2, the current model incorporates four jump processes: (i) Inception, (ii) Surface Reaction, (iii) Intra-particle Reaction and (iv) Coagulation. (Note: Sintering is described as a continuous process). A jump process m occurs with a probability given by:

$$P(m) = \frac{R_m(t)}{R_{\text{tot}}(t)}, \tag{87}$$

where $R_m(t)$ is the rate of process m at time t, $m \in \{\text{inc}, \text{coag}, \text{surf}, \text{int}\}$ and $R_{\text{tot}}(t)$ is the total rate of all jump processes calculated as:

$$R_{\text{tot}}(t) = R_{\text{inc}}(t) + R_{\text{coag}}(t) + R_{\text{surf}}(t) + R_{\text{int}}(t), \tag{88}$$

where the rates of individual processes at time t are given by (24), (36), (32) and (59).

The normalised frequency with which each type of jump event occurs is given by:

$$NN(m) = \frac{N_m(t)}{N_{\text{tot}}(t)}, \tag{89}$$

where $N_m(t)$ is the number of events of process m in a time-interval $[t-\tau, t]$ (τ is the waiting time), and $N_{\text{tot}}(t)$ is the total number of all jump processes occurring in a time-interval $[t-\tau, t]$:

$$N_{\text{tot}}(t) = N_{\text{inc}}(t) + N_{\text{coag}}(t) + N_{\text{surf}}(t) + N_{\text{int}}(t). \tag{90}$$

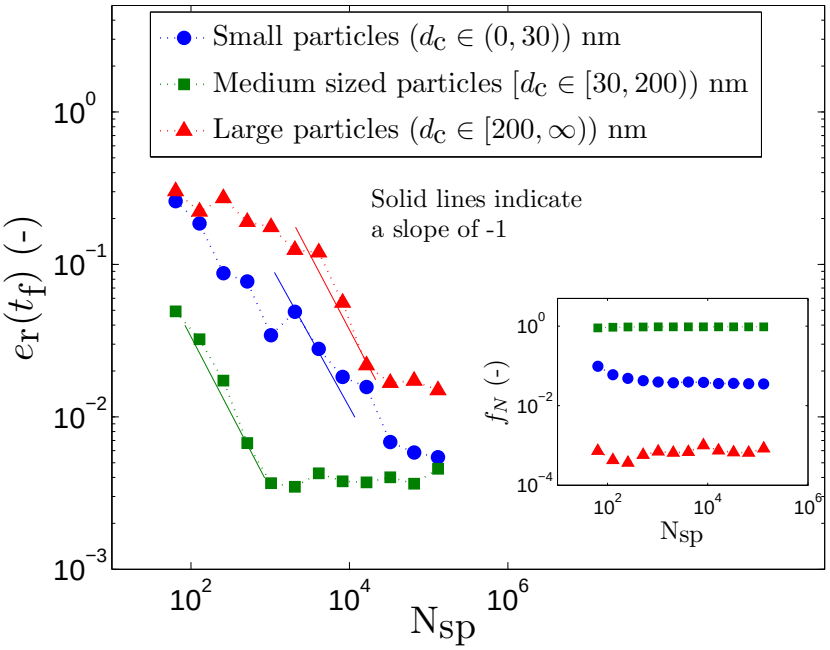

(a) *The relative error in sintering level at final time t_f conditioned on the basis of collision diameter. Inset depicts the fraction of particles in each size class.*

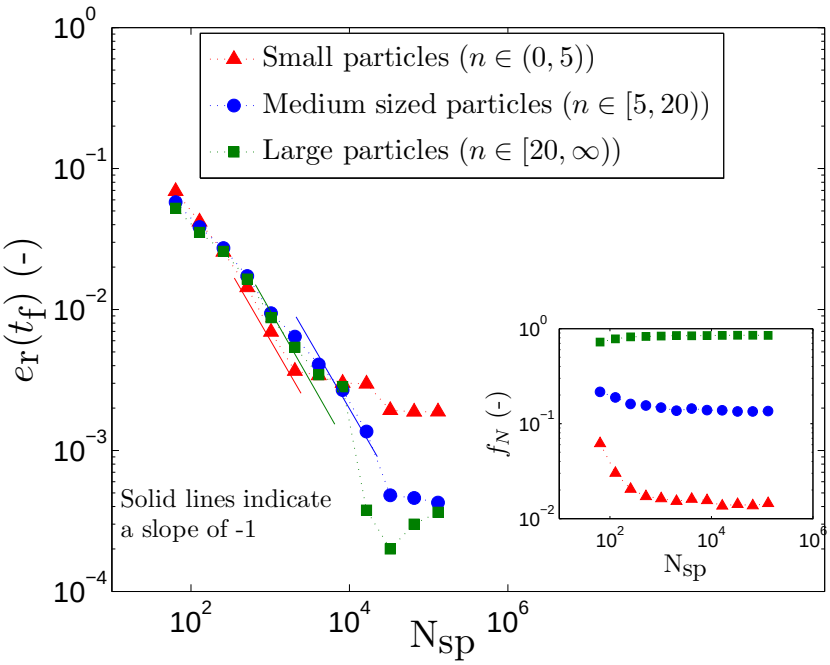

(b) *The relative error in Si:O ratio at final time t_f conditioned on the basis of number of primaries per particle. Inset depicts the fraction of particles in each size class.*

Figure 14: *Error in functionals conditioned on certain classes of values of another functional.*

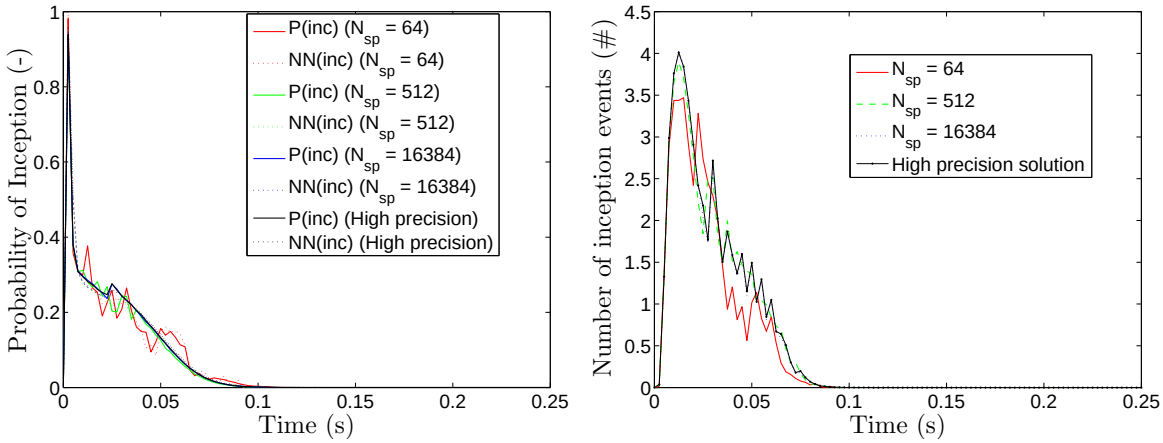

(a) *Probability of occurrence of inception calculated from the process rate P(inc) compared to the normalised number of inception events NN(inc).*

(b) *The absolute number of inception events normalised by N_{sp}.*

Figure 15: *Rates and jumps of inception events for the first 0.25 s.*

The quantity (89) is compared to the probability calculated from (87). **Figs. 15a-18a** depict the probability of the occurrence of a jump event calculated from rates $P(m)$ and the normalised frequency of each event $NN(m)$. **Figs. 15b-18b** present the absolute number of jump events normalised by the numerical parameter N_{sp}.

The probabilities of inception, surface reaction and intra-particle reaction decrease significantly after a short time of about 0.2 s. The reason for this is the dependence of these rates on the gas phase precursor concentration $C_{\text{Si(OH)}_4}$ as is evident from (24), (32) and (59). To analyse the behaviour of these rates, it is therefore important to study the the concentration of the gas-phase precursor.

The time profile of the gas-phase precursor (Si(OH)_4) concentration for the first 0.25 s is displayed in **Fig. 19a** for different values of N_{sp}. The inset in the main figure depicts the same quantity $C_{\text{Si(OH)}_4}$ on a logarithmic scale to highlight the observation that $C_{\text{Si(OH)}_4}$ does not entirely decay to zero after 0.1 s, but is present in very low concentrations of the order 10^{-15} to 10^{-20} mol/cm^3. **Fig. 19b** presents the evolution of the concentration of water ($C_{\text{H}_2\text{O}}$) for the first 0.25 s. Water is a by-product of all the particle processes (with the exception of coagulation) and hence its concentration increases with time.

The evolution of Si(OH)_4 takes place in three main phases:

(i) In the first phase, the gas-phase reactant TEOS is decomposed into Si(OH)_4. This phase is signified by the spike in the concentration of Si(OH)_4.

(ii) After 0.01 s, the Si(OH)_4 production process is completed. This is followed by the consumption of Si(OH)_4 by particle processes like inception and surface growth characterised by a drop in the concentration of Si(OH)_4.

(iii) The gas-phase precursor is completely consumed by particle processes after 0.1 s after which the concentration becomes small.

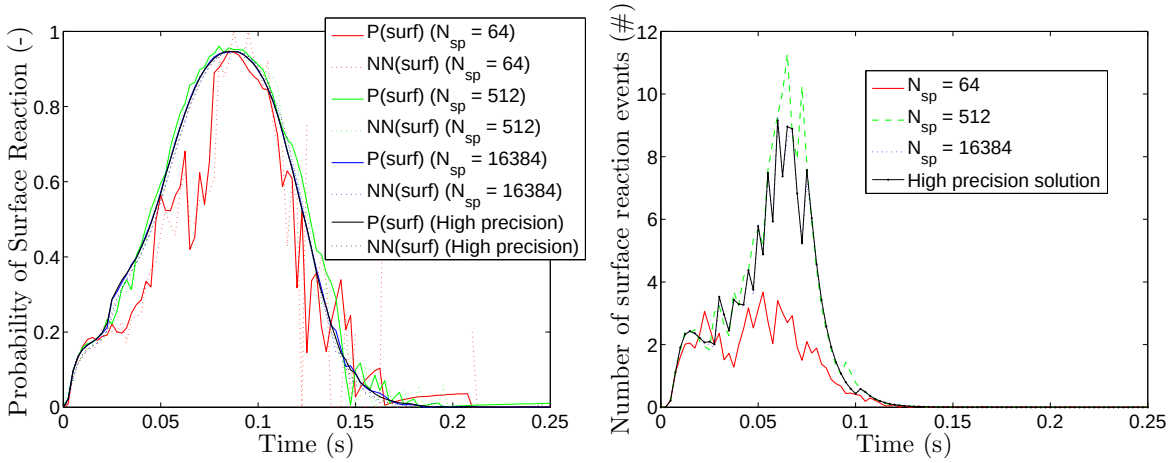

(a) *Probability of occurrence of surface reaction calculated from the process rate P(surf) compared to the normalised number of surface reaction events NN(surf).*

(b) *The absolute number of surface reaction events normalised by N_{sp}.*

Figure 16: *Rates and jumps of surface reaction events for the first 0.25 s.*

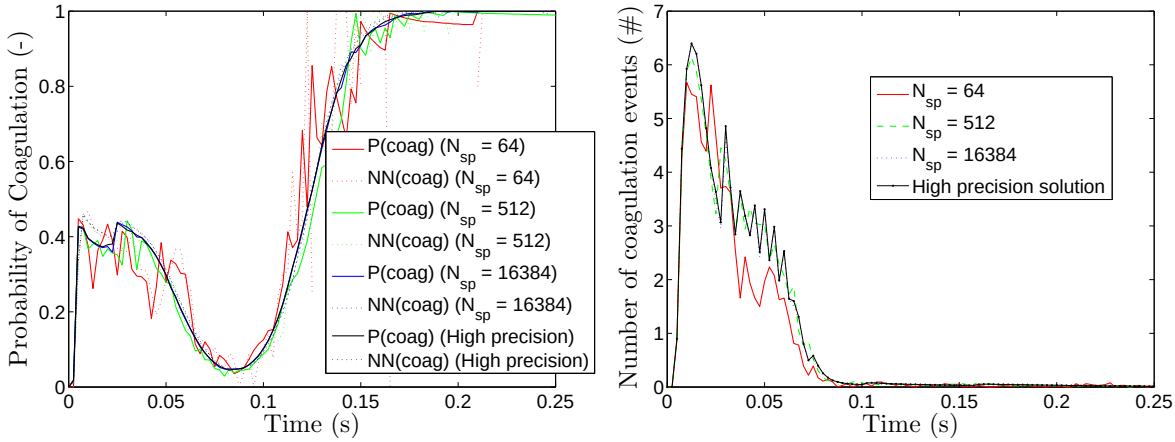

(a) *Probability of occurrence of coagulation calculated from the process rate P(coag) compared to the normalised number of coagulation events NN(coag).*

(b) *The absolute number of coagulation events normalised by N_{sp}.*

Figure 17: *Rates and jumps of coagulation events for the first 0.25 s.*

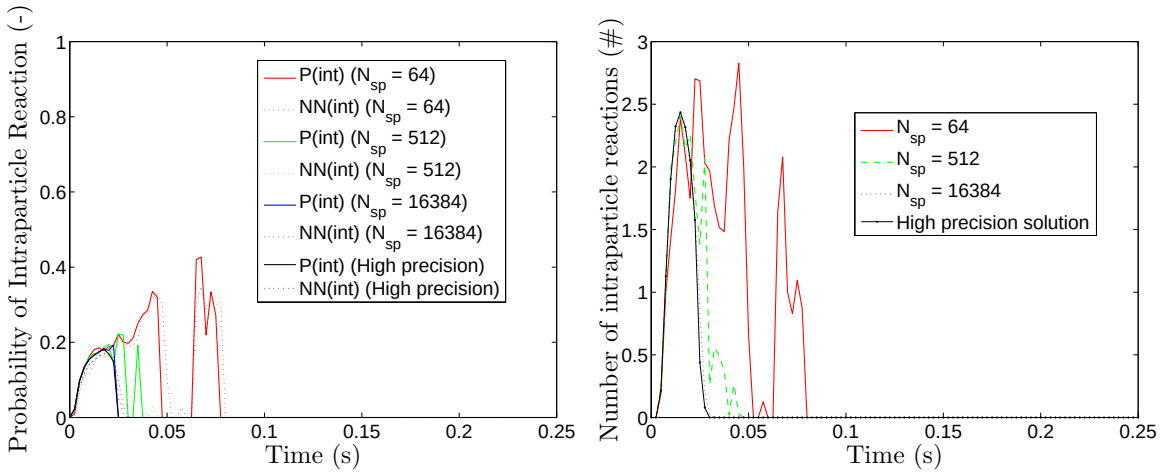

(a) *Probability of occurrence of intra-particle reaction calculated from the process rate P(int) compared to the normalised number of intra-particle reaction events NN(int).*

(b) *The absolute number of intra-particle reaction events normalised by N_{sp}.*

Figure 18: *Rates and jumps of intra-particle reaction events for the first 0.25 s.*

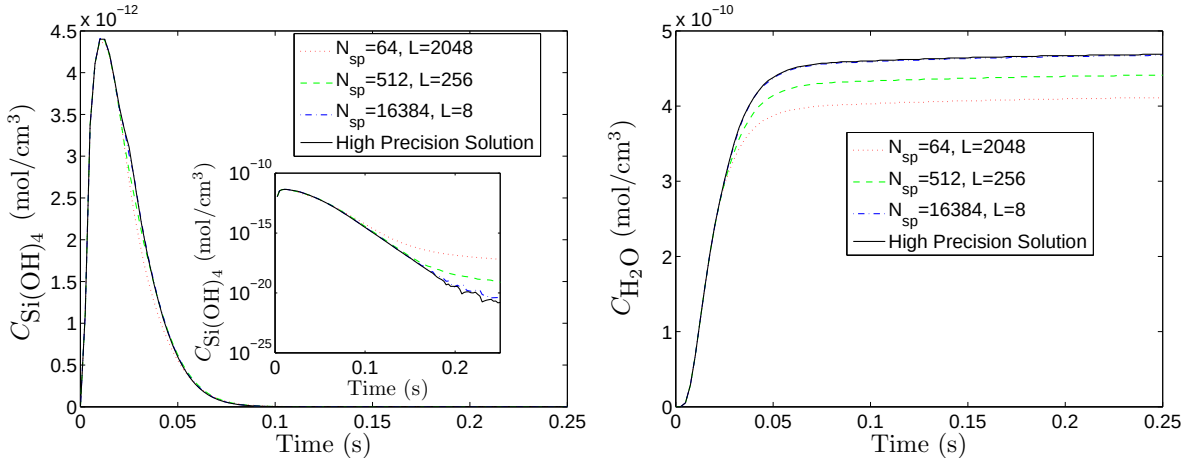

(a) *Time evolution of concentration of $Si(OH)_4$ for different N_{sp} for the first 0.25 s (Inset:Log-scale).*

(b) *Time evolution of concentration of H_2O for different N_{sp} for the first 0.25 s.*

Figure 19: *Cumulative number of particle jump events for different N_{sp}.*

As shown in Fig. 19a, $C_{\mathrm{Si(OH)_4}}$ decays in a relatively short time (≈ 0.1 s). The inception rate (24) shows a second order dependence on the quantity $C_{\mathrm{Si(OH)_4}}$ and therefore shows immediate response to the decrease in the value of $C_{\mathrm{Si(OH)_4}}$. The surface reaction rate, however, is also a function of the state space variable η_{OH} in addition to $C_{\mathrm{Si(OH)_4}}$. After 0.1 s, although the value of $C_{\mathrm{Si(OH)_4}}$ is of the order 10^{-15} mol/cm^3, the value of η_{OH} is sufficiently high to result in a significant value of surface reaction rate until about 0.2 s. The quantity (32) thus shows a delayed response to the value of $C_{\mathrm{Si(OH)_4}}$.

It is inferred from Figs. 15a-18a that as the number of stochastic particles (N_{sp}) is increased, the normalised frequencies and probabilities calculated using rates converge to

each other. The absolute number of jump events (Figs. 15b-18b) are also observed to converge with increasing values of N_{sp}.

3.3.3 Computational Efficiency

The simulation computational times (CT) for different values of the numerical parameter N_{sp} are presented in **Fig. 20**. The computational time is observed to increase with increasing N_{sp}.

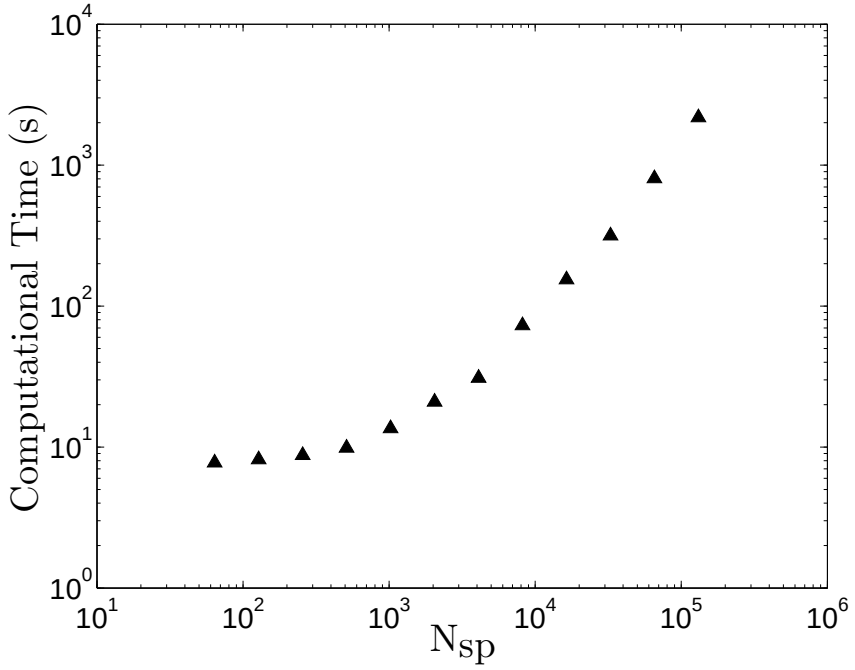

Figure 20: *Computational times as a function of number of stochastic particles.*

The relative convergence speed of different functionals was investigated by comparing the relative errors (80) as a function of N_{sp} as depicted in **Fig. 21**. It is observed that the zeroth moment M_0 was the fastest to converge with a low relative error of 1% attained in ≈ 15 s. Collision diameter D_{c} converges in ≈ 30 s, whilst the ensemble volume-fraction F_{v} is the slowest, taking almost ten times as long as M_0 to converge. The study of relative convergence speeds of different functionals motivates the choice of appropriate values of the numerical parameters in order to obtain a desired accuracy in a specific functional for a prescribed computational time.

3.3.4 Convergence with respect to Δt_{s}

A brief convergence study of three functionals (84), (85) and (86) is performed with respect to the splitting time step to ensure that this was chosen sufficiently small to obtain a reasonably converged solution. From Fig. 19a, it is observed that the gas-phase reactant species attains full conversion to particle phase in 0.1 s. The necessity of having a small

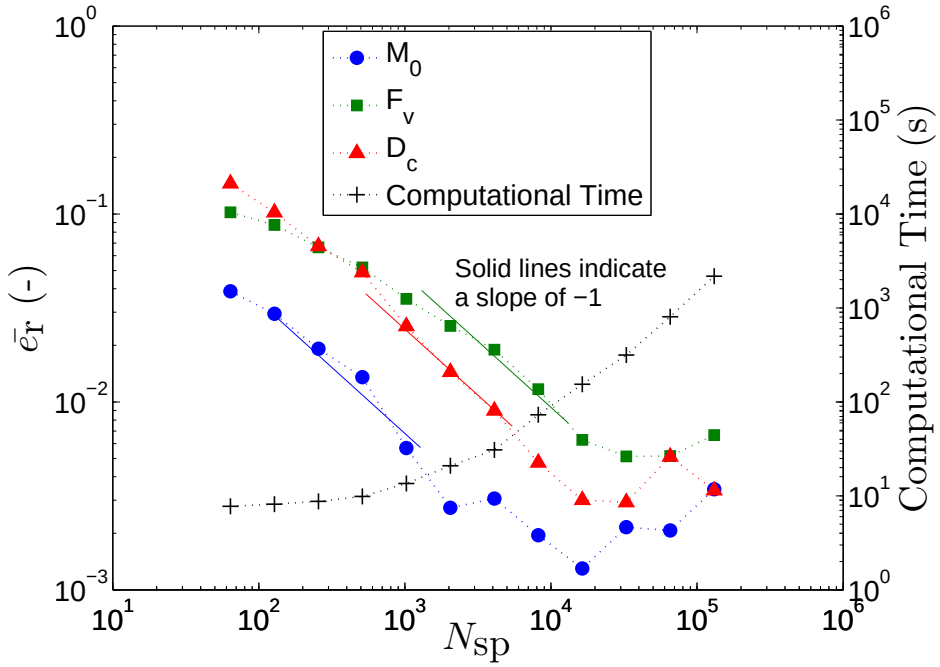

Figure 21: *Relative convergence speeds of different functionals.*

splitting time step therefore lies in the initial time period when the concentration gradients are large.

To study the convergence behaviour with respect to Δt_s, we vary the splitting time step for the first 0.25 s of the reactor residence time. All calculations are performed at sufficiently high value of N_{sp} and L to minimise errors.

The time profiles for quantities (84), (85) and (86) for different values of the splitting time step are given in **Fig. 22a**, **Fig. 22c** and **Fig. 22e** respectively. The corresponding values of quantity (83) for these functionals are is given in **Fig. 22b**, **Fig. 22d** and **Fig. 22f**. These functionals are observed to converge rapidly as Δt_s is reduced.

4 Conclusion

This work investigates the numerical aspects of a detailed multivariate population balance model to study the structure and composition of silica nanoparticles formed from TEOS by thermal decomposition. A mathematical statement of the model is presented where each particle is represented in terms of its primary particles and the connectivity between these primaries. Each primary particle, in turn, is described by its chemical composition *i.e.*, the number of Si, O and OH groups present within it. The particles transform in their type space due to different particle processes such as surface reaction, coagulation, sintering, and intra-particle processes; the rates and transformations associated with these processes are presented. The algorithms used to solve the population balance equations

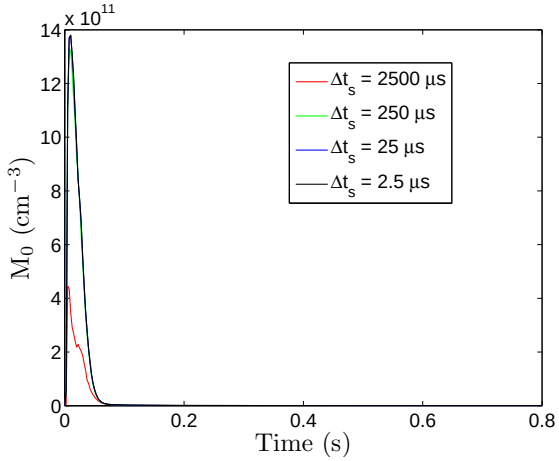

(a) *Time evolution of M_0 for different Δt_s.*

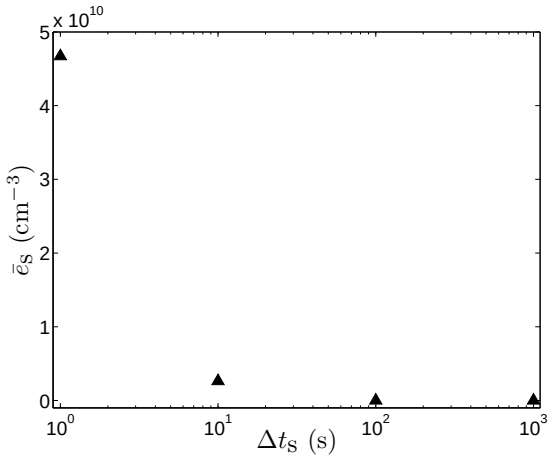

(b) *Average error $\bar{e}_s$ in M_0 for different Δt_s.*

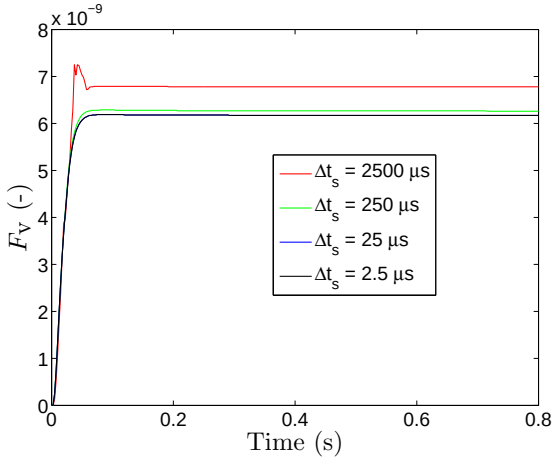

(c) *Time evolution of F_v for different Δt_s.*

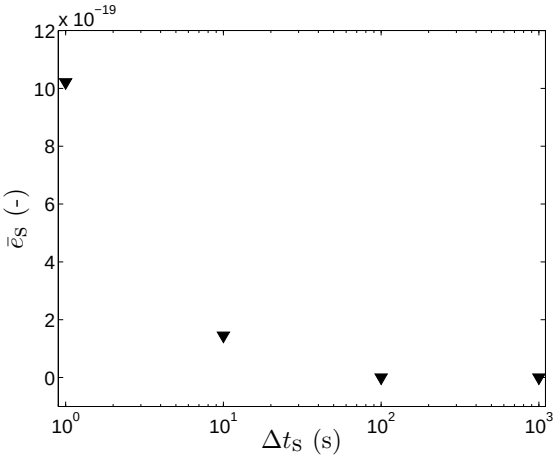

(d) *Average error $\bar{e}_s$ in V for different Δt_s.*

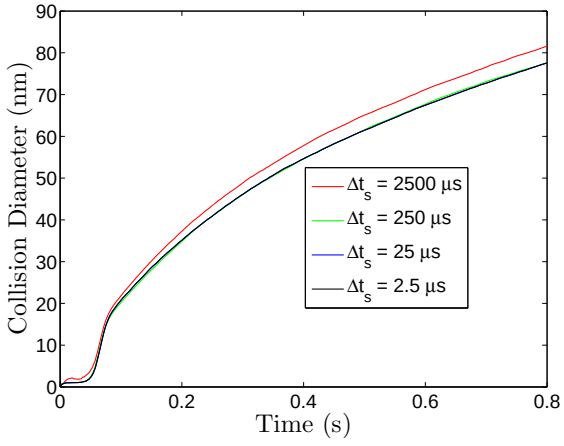

(e) *Time evolution of D_c for different Δt_s.*

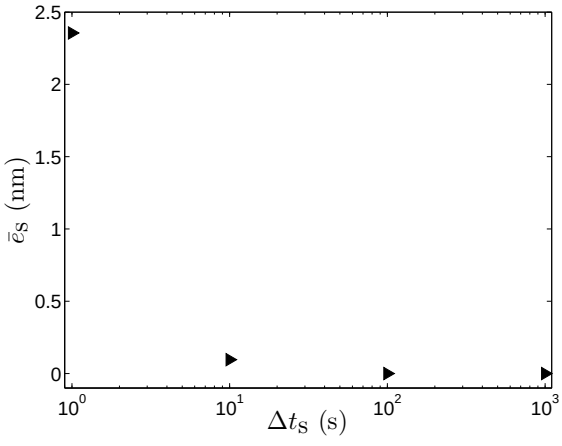

(f) *Average error in $\bar{e}_s$ in D_c for different Δt_s.*

Figure 22: *Time evolution and average errors of various functionals for different splitting time steps.*

and the operator splitting technique to couple the solution of the PBEs with a gas-phase chemistry solver have been described.

A detailed numerical study of the model has been performed with respect to the numerical parameter that determines the number of computational particles in the system. The convergence behaviour of various functionals are observed and whilst a fast convergence order of $\sim 1/N_{\text{sp}}$ is achieved for the zeroth moment (particle number density), volume-fraction and collision diameter of the ensemble, the convergence of higher order functionals (for *e.g.* , sintering level) are observed to be slower. The computational efficiency of the algorithm has also been reported. Finally, a brief numerical study with respect to another numerical parameter of the model, the splitting time step, is performed to ensure the splitting time step was chosen adequately to obtain a converged solution.

The current study presents the mathematical formulation of a novel population balance model to describe nanoparticle dynamics in an unprecedented level of detail. An elaborate numerical treatment of this model has been explored. The low CPU times indicate the potential for coupling this model with computational fluid dynamics (CFD) codes to bridge the gap between micro and macroscopic scales and therefore facilitate the simulation of industrial flow reactors. This work demonstrates the feasibility of using a multidimensional approach to understand complex nanoparticle systems.

5 Acknowledgements

The authors acknowledge financial support provided by HeiQ materials. SS is thankful to the Cambridge Commonwealth Trust and Murray Edwards BP Centenary bursary for funding her PhD. MK is grateful for the support of the Weierstrass Institute for Applied Analysis and Stochastics (WIAS) in Berlin. The authors also thank members of the Computational Modelling Group for their support.

A Appendix

A.1 Derivation of rate of intra-particle reaction.

The chemical units in particle P_q vary with time t. After a time interval of Δt, the following events happen to change the type space of P_q :

1. Let the average number of surface reaction events that occur in Δt be $N_{\text{surf}}(P_q)$.
2. Let the average number of intra-particle events that occur in Δt be $N_{\text{int}}(P_q)$.
3. Let the average number of OH units that are reduced by sintering in time Δt be $\Delta_{\text{sint}}\eta_{\text{OH}}(P_q)$.

Using the relevant jumps defined in §2.2.2 associated with each of these processes, we get the changes in Si,O and OH units of P_q as:

$$\Delta\eta_{\text{Si}}(P_q) = N_{\text{surf}},$$

$$\Delta\eta_{\text{O}}(P_q) = N_{\text{surf}} + N_{\text{int}} + \frac{\Delta_{\text{sint}}\eta_{\text{OH}}(P_q)}{2},$$

$$\Delta\eta_{\text{OH}}(P_q) = 2N_{\text{surf}} - 2N_{\text{int}} - \Delta_{\text{sint}}\eta_{\text{OH}}(P_q).$$

The total change in O units of the particle is given by the sum of change in free O units ($\Delta\eta_{\text{O}}(P_q)$) and those in OH units ($\Delta\eta_{\text{OH}}(P_q)$). Thus, $\Delta\eta_{\text{O,total}}(P_q) = \Delta\eta_{\text{O}}(P_q) + \Delta\eta_{\text{OH}}(P_q)$. The ratio of Si to O is thus given by:

$$\frac{\Delta\eta_{\text{Si}}(P_q)}{\Delta\eta_{\text{O,total}}(P_q)} = \frac{N_{\text{surf}}}{3N_{\text{surf}} - N_{\text{int}} - \frac{\Delta_{\text{sint}}\eta_{\text{OH}}(P_q)}{2}}. \tag{A.1}$$

The stochiometric ratio of Si:O in particle P_q has to be 1:2. By assuming the number of events of each process are much greater than the initial number of Si, O and OH in P_q, substituting in (A.1) we get,

$$\frac{N_{\text{surf}}}{3N_{\text{surf}} - N_{\text{int}} - \frac{\Delta_{\text{sint}}\eta_{\text{OH}}(P_q)}{2}} := \frac{1}{2} \tag{A.2}$$

$$\implies N_{\text{int}} = N_{\text{surf}} - \frac{\Delta_{\text{sint}}\eta_{\text{OH}}(P_q)}{2}. \tag{A.3}$$

Dividing (A.3) by Δt, we get:

$$R_{\text{int}} = R_{\text{surf}} - \frac{\Delta_{\text{sint}}\eta_{\text{OH}}(P_q)}{2\Delta t}. \tag{A.4}$$

As discussed in §2.2.2, the surface density of OH sites is assumed to be constant throughout the sintering process. The reduction in surface area due to sintering is thus accompanied by a reduction in the number of OH sites. The change in number of OH in particle P_q due to sintering is given by:

$$\frac{\Delta_{\text{sint}}\eta_{\text{OH}}(P_q)}{2\Delta t} = \frac{\rho_{\text{s}}(P_q)}{2}\frac{\Delta S(P_q)}{\Delta t}, \tag{A.5}$$

where $\Delta S(P_q)$ is the net change in surface of P_q due to sintering and $\rho_{\text{s}}(P_q) = \eta_{\text{OH}}(P_q)/S(P_q)$ is the surface density of OH sites. Since the change in surface area of P_q is the sum of change of surface areas of all its constituent primaries, we get:

$$\frac{\Delta S(P_q)}{\Delta t} = \sum_{i,j=1}^{n(P_q)} \frac{\Delta C_{ij}}{\Delta t}. \tag{A.6}$$

Substituting the value of rate of change of surface ($\Delta C_{ij}/\Delta t$) from (40), we get the overall rate of intra-particle reaction for particle P_q as:

$$R_{\text{int}}(P_q) = A_{\text{surf}} \exp\left(-\frac{E_{\text{a}}}{RT}\right)\eta_{\text{OH}}(P_q)N_{\text{A}}C_{\text{Si(OH)}_4} - \frac{\rho_{\text{s}}(P_q)}{2}\left[\sum_{i,j=1}^{n(P_q)} \frac{C_{ij} - S_{\text{sph}}(p_i,p_j)}{\tau(p_i,p_j)}\right]. \tag{A.7}$$

A.2 Bounds for sintering level

Sintering level $s(p_i, p_j)$ between two primaries p_i and p_j quantifies the extent of sintering between them.

$$s(p_i,p_j) = \frac{\frac{S_{\text{sph}}(p_i,p_j)}{C_{ij}} - 2^{-\frac{1}{3}}}{1 - 2^{-\frac{1}{3}}}. \tag{A.8}$$

Lower Bound

The lower bound of sintering level is calculated when the two primaries are in point contact. Thus:

$$C_{ij} = \pi(d_p(p_i)^2 + d_p(p_j)^2) \tag{A.9}$$

$S_{\text{sph}}(p_i, p_j)$ is the surface area of a sphere with the same volume as that of primaries p_i and p_j.

$$S_{\text{sph}}(p_i,p_j) = \pi(d_p(p_i)^3 + d_p(p_j)^3)^{\frac{2}{3}} \tag{A.10}$$

$d_p(p_i)$ and $d_p(p_j)$ are the diameters of primary particles p_i and p_j.

$$s(p_i,p_j)^{\text{LB}} = \frac{\frac{\pi(d_p(p_i)^3+d_p(p_j)^3)^{\frac{2}{3}}}{\pi(d_p(p_i)^2+d_p(p_j)^2)} - 2^{-\frac{1}{3}}}{1-2^{-\frac{1}{3}}}. \tag{A.11}$$

Let us assume that $d_p(p_i) = \alpha d_p(p_j)$, where α is some constant. Substituting we get:

$$s(p_i,p_j)^{\text{LB}} = \frac{\frac{(1+\alpha^3)^{\frac{2}{3}}}{1+\alpha^2} - 2^{-\frac{1}{3}}}{1-2^{-\frac{1}{3}}}. \tag{A.12}$$

$$s(p_i,p_j)^{\text{LB}} = \begin{cases} 0, \text{ if } \alpha = 1 (\text{two primaries of equal size}), \\ > 0, \text{ if } \alpha \neq 1. \end{cases} \tag{A.13}$$

Upper Bound

The upper bound of sintering level is calculated when two primaries are completely sintered and spherical. Thus:

$$C_{ij} = S_{\text{sph}}(p_i,p_j) = \pi(d_p(p_i)^3 + d_p(p_j)^3)^{\frac{2}{3}} \tag{A.14}$$

Thus $s(p_i,p_j)^{\text{UB}}$ is given by:

$$s(p_i,p_j)^{\text{UB}} = \frac{\frac{C_{ij}^{\text{UB}}}{S_{\text{sph}}(p_i,p_j)} - 2^{-\frac{1}{3}}}{1-2^{-\frac{1}{3}}} = 1. \tag{A.15}$$

We conclude that:

$$0 \leq s(p_i,p_j) \leq 1. \tag{A.16}$$

References

[1] M. Balthasar and M. Kraft. A stochastic approach to solve the particle size distribution function of soot particles in laminar premixed flames. *Combustion and Flame*, 133:289–298, 2003. doi:10.1016/S0010-2180(03)00003-8.

[2] M. S. Celnik, R. I. A. Patterson, M. Kraft, and W. Wagner. Coupling a stochastic soot population balance to gas-phase chemistry using operator splitting. *Combustion and Flame*, 148(3):158–176, 2007. doi:10.1016/j.combustflame.2006.10.007.

[3] M. S. Celnik, A. Raj, R. H. West, R. I. A. Patterson, and M. Kraft. An aromatic site description of soot particles. *Combustion and Flame*, 155(1-2):161–180, 2008. doi:10.1016/j.combustflame.2008.04.011.

[4] M. S. Celnik, R. I. A. Patterson, , M. Kraft, and W. Wagner. A predictor-corrector algorithm for the coupling of stiff odes to a particle population balance. *Journal of Computational Physics*, 228(8):2758–2769, 2009. doi:10.1016/j.jcp.2008.12.030.

[5] A. Eibeck and W. Wagner. An efficient stochastic algorithm for studying coagulation dynamics and gelation phenomena. *SIAM Journal on Scientific Computing*, 22(3): 802–821, 2000. doi:10.1137/S1064827599353488.

[6] M. Goodson and M. Kraft. An efficient stochastic algorithm for simulating nanoparticle dynamics. *Journal of Computational Physics*, 183(1):210–232, 2002. doi:10.1006/jcph.2002.7192.

[7] P. Ho and C. F. Melius. Theoretical study of the thermochemistry of molecules in the Si-C-H-C system. *Journal of Physical Chemistry*, 99:2166–2176, 1995. doi:10.1021/j100007a056.

[8] H. M. Hulburt and S. Katz. Some problems in particle technology: A statistical mechanical formulation. *Chemical Engineering Science*, 19(8):555–574, 1964. doi:10.1016/0009-2509(64)85047-8.

[9] W. Koch and S. K. Friedlander. The effect of particle coalescence on the surface area of a coagulating aerosol. *Journal of Colloid and Interface Science*, 140(2):73–76, 1990. doi:10.1016/0021-9797(90)90362-R.

[10] W. Koch and S. K. Friedlander. Particle growth by coalescence and agglomeration. *Journal of aerosol science*, 21(1):419–427, 1990. doi:10.1016/0021-8502(90)90192-Z.

[11] M. Kraft. Modelling of particulate processes. *Kona, Powder and Particle*, 23, 2005. URL `http://www.kona.or.jp/pdf/2005.pdf#page=19`.

[12] B. W. Lee, J. I. Jeong, J. Y. Hwang, M. Choi, and S. H. Chung. Analysis of growth of non-spherical silica particles in a counterflow diffusion flame considering chemical reactions, coagulation and coalescence. *Journal of Aerosol Science*, 32(2):165–185, 2001. doi:10.1016/S0021-8502(00)00054-9.

[13] N. Morgan, C. Wells, M. Kraft, and W. Wagner. Modelling nanoparticle dynamics: Coagulation, sintering, particle inception and surface growth. *Combustion Theory and Modelling*, 9(3):449–461, 2005. doi:10.1080/13647830500277183.

[14] N. Morgan, M. Kraft, M. Balthasar, D. Wong, M. Frenklach, and P. Mitchell. Numerical simulations of soot aggregation in premixed laminar flames. *Proceedings of the Combustion Institute*, 31:693–700, 2007. doi:10.1016/j.proci.2006.08.021.

[15] R. Mueller, H. K. Kammler, S. E. Pratsinis, A. Vital, G. Beaucage, and P. Burtscher. Non-agglomerated dry silica nanoparticles. *Powder Technology*, 140(1-2):40–48, 2004. doi:10.1016/j.powtec.2004.01.004.

[16] R. I. A. Patterson and M. Kraft. Models for the aggregate structure of soot particles. *Combustion and Flame*, 151:160–172, 2007. doi:10.1016/j.combustflame.2007.04.012.

[17] R. I. A. Patterson, J. Singh, M. Balthasar, M. Kraft, and W. Wagner. Extending stochastic soot simulation to higher pressures. *Combustion and Flame*, 145(3):638–642, 2006. doi:10.1016/j.combustflame.2006.02.005.

[18] W. Phadungsukanan, S. Shekar, R. Shirley, M. Sander, R. H. West, and M. Kraft. First-principles thermochemistry for silicon species in the decomposition of tetraethoxysilane. *Journal of Physical Chemistry A*, 113:9041–9049, 2009. doi:10.1021/jp905494s.

[19] D. Ramkrishna and A. W. Mahoney. Population balance modeling. Promise for the future. *Chemical Engineering Science*, 57(4):595–606, 2002. doi:10.1016/S0009-2509(01)00386-4.

[20] K. K. Sabelfeld, S. V. Rogasinsky, A. A. Kolodko, and A. I. Levykin. Stochastic algorithms for solving smolouchovsky coagulation equation and applications to aerosol growth simulation. *Monte Carlo Methods and Applications*, 2(1):41–87, 1996. doi:10.1515/mcma.1996.2.1.41.

[21] M. Sander, R. I. A. Patterson, A. Braumann, A. Raj, and M. Kraft. Developing the pah-pp soot particle model using process informatics and uncertainty propagation. *Proceedings of the Combustion Institute*, 33:675683, 2011. doi:10.1016/j.proci.2010.06.156.

[22] T. Seto, A. Hirota, T. Fujimoto, M. Shimada, and K. Okuyama. Sintering of Polydisperse Nanometer-Sized Agglomerates. *Aerosol Science and Technology*, 27(3): 422–438, 1997. doi:10.1080/02786829708965482.

[23] S. Shekar, M. Sander, R. Shaw, A. J. Smith, A. Braumann, and M. Kraft. Modelling the flame synthesis of silica nanoparticles from tetraethoxysilane. *Chemical Engineering Science*, In Press, 2011. doi:10.1016/j.ces.2011.06.010.

[24] S. Shekar, A. J. Smith, W. Menz, M. Sander, and M. Kraft. A multidimensional population balance model to describe the aerosol synthesis of silica nanoparticles. Technical Report 103, c4e Preprint-Series, Cambridge, 2011. URL como.cheng.cam.ac.uk/preprints/c4e-Preprint-103.pdf. Submitted to *Journal of Aerosol Science*.

[25] G. Strang. On the construction and comparison of difference schemes. *SIAM Journal on Numerical Analysis*, 5(3):506–517, 1968. URL http://www.jstor.org/stable/2949700.

[26] S. Tsantilis, H. Briesen, and S. E. Pratsinis. Sintering time for silica particle growth. *Aerosol Science and Technology*, 34(3):237–246, 2001. doi:10.1080/02786820119149.

[27] S. Tsantilis, H. K. Kammler, and S. E. Pratsinis. Population balance modeling of flame synthesis of titania nanoparticles. *Chemical Engineering Science*, 57(12): 2139–2156, 2002. doi:10.1016/S0009-2509(02)00107-0.

[28] G. D. Ulrich. Theory of particle formation and growth in oxide synthesis flames. *Combustion Science and Technology*, 4(1):47–57, 1971. doi:10.1080/00102207108952471.

[29] G. D. Ulrich and J. W. Riehl. Aggregation and growth of submicron oxide particles in flames. *Journal of Colloid and Interface Science*, 87(1):257–265, 1982. doi:10.1016/0021-9797(82)90387-3.

[30] R. H. West, M. S. Celnik, O. R. Inderwildi, M. Kraft, G. J. O. Beran, and W. H. Green. Towards a comprehensive model of the synthesis of TiO_2 particles from $TiCl_4$. *Industrial and Engineering Chemistry Research*, 46(19):6147–6156, 2007. doi:10.1021/ie0706414.

[31] Y. Xiong and S. E. Pratsinis. Formation of agglomerate particles by coagulation and sintering-Part I: A two-dimensional solution of the population balance equation. *Journal of Aerosol Science*, 24(3):283300, 1993. doi:10.1016/0021-8502(93)90003-R.

[32] Y. Xiong, M. K. Akhtar, and S. E. Pratsinis. Formation of agglomerate particles by coagulation and sintering-Part II: The evolution of the morphology of aerosol-made titania, silica and silica-doped titania powders. *Journal of Aerosol Science*, 24(3): 301313, 1993. doi:10.1016/0021-8502(93)90004-S.

Citation index